nature cell biology

ARTICLES

https://doi.org/10.1038/s41556-018-0091-6

XMAP215 is a microtubule nucleation factor that functions synergistically with the γ-tubulin ring complex

Akanksha Thawani[1,3], Rachel S. Kadzik[2,3] and Sabine Petry[2]*

How microtubules (MTs) are generated in the cell is a major question in understanding how the cytoskeleton is assembled. For several decades, γ-tubulin has been accepted as the universal MT nucleator of the cell. Although there is evidence that γ-tubulin complexes are not the sole MT nucleators, identification of other nucleation factors has proven difficult. Here, we report that the well-characterized MT polymerase XMAP215 (chTOG/Msps/Stu2p/Alp14/Dis1 homologue) is essential for MT nucleation in *Xenopus* egg extracts. The concentration of XMAP215 determines the extent of MT nucleation. Even though XMAP215 and the γ-tubulin ring complex (γ-TuRC) possess minimal nucleation activity individually, together, these factors synergistically stimulate MT nucleation in vitro. The amino-terminal TOG domains 1–5 of XMAP215 bind to αβ-tubulin and promote MT polymerization, whereas the conserved carboxy terminus is required for efficient MT nucleation and directly binds to γ-tubulin. In summary, XMAP215 and γ-TuRC together function as the principal nucleation module that generates MTs in cells.

Microtubules (MTs) form various cytoskeletal structures that are vital to the function of the cell, including the mitotic spindle. The first step in building these structures is the generation of MTs; yet, little is known about how MTs are nucleated in the cell. MTs can assemble spontaneously in vitro from high concentrations of αβ-tubulin dimers[1]. By contrast, spontaneous MT formation rarely occurs in vivo. Instead, MTs are nucleated at specific sites termed MT-organizing centres (MTOCs)[2,3]. Essential to all MTOCs is the protein γ-tubulin, which is widely accepted as the cell's universal MT nucleator[3,4]. γ-Tubulin forms a complex with γ-tubulin complex proteins (GCPs) and assembles into the γ-tubulin ring complex (γ-TuRC)[5–7]. γ-TuRC positions an outer ring of approximately 13 γ-tubulin molecules, which are thought to interface with α-tubulin subunits and thereby provide a template for MT assembly[7–10]. However, this model for MT nucleation remains to be experimentally tested.

There is growing evidence that γ-TuRC alone does not account for all the MT nucleation activity in the cell. In the absence of γ-TuRC, MTs still form, albeit with substantially reduced numbers and kinetics[11–13]. In addition, at least one factor of unknown identity besides γ-TuRC is needed to promote nucleation from centrosomes[14]. Furthermore, purified γ-tubulin complexes display low nucleation potential in vitro[5,7,9,14–18] that does not match the nucleation activity observed from cellular MTOCs. Together, these data indicate that the current γ-TuRC-centred model of MT nucleation is incomplete. Thus, the search for factors that generate MTs in the cell is ongoing, and how MT nucleation occurs remains to be elucidated.

After their nucleation, growth of MTs is necessary for building cytoskeletal structures. The major MT polymerase in the cell, XMAP215, increases polymerization rates up to tenfold in vitro and in vivo[19–28]. XMAP215 is a multi-domain protein consisting of five tumour-overexpressed gene (TOG) domains at the amino terminus and a carboxy-terminal domain[23]. The TOG domains bind to soluble αβ-tubulin dimers[22,29,30] and are essential for the polymerase activity of XMAP215 (ref. [24]). Recently, TOG4 and TOG5 domains have been suggested to interact with αβ-tubulin incorporated in the MT lattice[31]. Although primarily characterized as a polymerase, XMAP215, similar to several other MT-associated proteins, promotes spontaneous MT assembly[27,29,32] and re-growth from MT templates in vitro[33]. However, a mass balance model of the mitotic spindle suggested that XMAP215 only enhances growth of individual MTs and does not influence their nucleation[26]. Thus, it remains unclear whether XMAP215 is involved in nucleating MTs in the cytoplasm because assays to visualize nucleation events in the cell are lacking. Furthermore, if XMAP215 were to function as a MT nucleator, its relationship with the universal nucleator γ-TuRC needs to be established and their mechanism determined[27,34,35].

In this study, we demonstrate that XMAP215 is a bona fide MT nucleation factor that cooperates with γ-TuRC. Using *Xenopus* egg extracts to resolve individual nucleation events, we show that XMAP215 determines the extent of MT nucleation in the cytoplasm. XMAP215 and γ-TuRC operate synergistically to generate MTs in vitro, and the C terminus of XMAP215 is required for this cooperation. We further demonstrate that XMAP215 directly interacts with γ-tubulin via its C terminus. Thus, XMAP215 is a major MT nucleation factor that functions with γ-TuRC to give rise to the MT cytoskeleton.

Results

XMAP215 is required for MT nucleation. To investigate how MT structures are built via MT nucleation, we used a system that allows visualization of individual MT nucleation events in the cytoplasm. Specifically, we studied what role the polymerase XMAP215 has in generating branched, fan-like MT structures in *Xenopus* egg extracts induced by the dominant active form of the small GTPase Ran (RanQ69L)[36]. We visualized MT nucleation from pre-existing MTs using time-lapse total internal reflection fluorescence (TIRF) microscopy with Cy5-labelled MTs and mCherry-labelled end-binding protein 1 (EB1) to highlight the growing MT plus ends (Supplementary Fig. 1a).

[1]Department of Chemical and Biological Engineering, Princeton University, Princeton, NJ, USA. [2]Department of Molecular Biology, Princeton University, Princeton, NJ, USA. [3]These authors contributed equally: Akanksha Thawani and Rachel S. Kadzik. *e-mail: spetry@princeton.edu

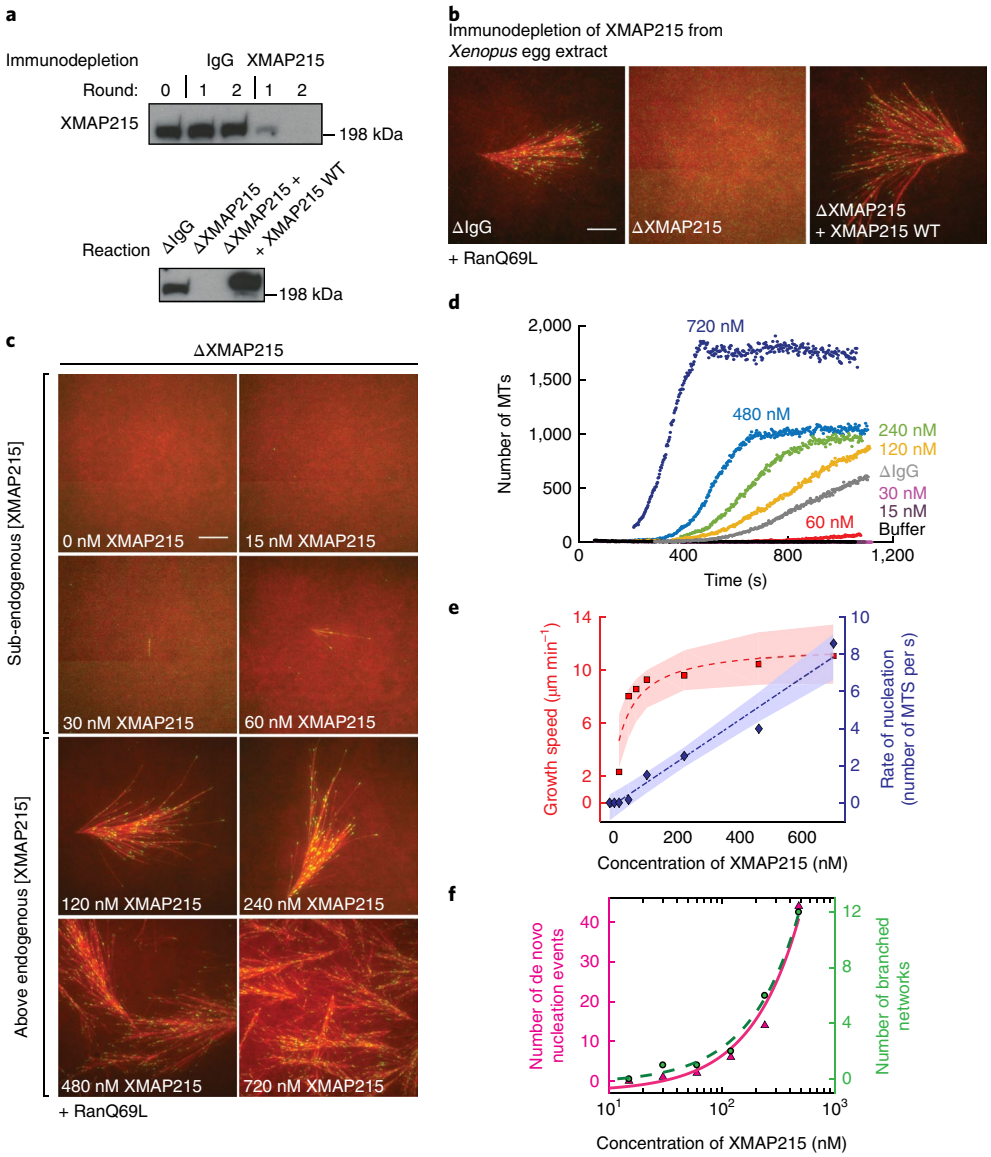

Fig. 1 | XMAP215 stimulates MT nucleation in *Xenopus* egg extracts. a,**b**, Western blot analysis of XMAP215 or IgG immunodepletion from *Xenopus* extracts and add-back of wild-type (WT) XMAP215-GFP, probed using an antibody against the TOG12 domain. Branching MT nucleation was induced in *Xenopus* extracts in the presence of 5.5 μM RanQ69L (**b**). EB1-mCherry (pseudocoloured as green) and Cy5-labelled tubulin (red) were added. XMAP215-GFP was added back at 85 nM (equivalent to 120 nM in IgG-depleted extracts). Representative images are displayed at 20 minutes of the reaction. Scale bar, 10 μm. The experiments were repeated at least three times with independent extract preparations. **c**, Increasing concentration of XMAP215-GFP added back to the immunodepleted extracts with 5.5 μM RanQ69L. Representative images are displayed at 480 seconds. Scale bar, 10 μm. See Supplementary Video 2. The experiment was repeated four times with independent extract preparations. **d**, EB1 comets in the entire field of view were detected, counted and plotted over time. **e**, Growth speed of MTs was obtained by tracking all EB1 comets observed during the experiment. No MTs nucleated below 30 nM XMAP215 and growth speed was not measured. At 30 nM, growth speed was measured manually as $2.3 \pm 0.8\ \mu m\ min^{-1}$ (mean ± s.d.; $n = 25$). For ≥60 nM, growth speed was computed via image analysis: 60 nM: 8.0 ± 1.9 ($n = 1{,}470$), 85 nM: 8.5 ± 1.8 nM ($n = 18{,}190$), 120 nM: 9.3 ± 2.0 ($n = 45{,}090$), 240 nM: 9.6 ± 2.2 ($n = 59{,}297$), 480 nM: 10.5 ± 2.4 ($n = 79{,}381$) and 720 nM: $11.1 \pm 2.7\ \mu m\ min^{-1}$ ($n = 147{,}008$). *n* represents the number of growth speed measurements obtained from consecutive frames of all tracks. Mean speed (red squares) versus concentration was fit to Michaelis–Menten kinetics (red dashed line). Rate of nucleation (blue diamonds) was measured as the slope of the linear region of nucleation curves in **d**. Rate of nucleation versus concentration was regressed to a straight line (blue dashed line). 95% confidence intervals of the fits are shaded. **f**, De novo nucleation events and branched networks that emerged were counted manually for each reaction (magenta triangles and green circles, respectively). Linear fit to each is plotted as solid and dashed curves. The *x* axis is displayed in log scale, where the concentration of 0 nM cannot be shown (green circles). The analyses in **d**–**f** were repeated at least three times with independent extract preparations. See Supplementary Figs. 1 and 9, Supplementary Video 1 and Supplementary Table 2 for source data.

To assess the role of XMAP215, we first added recombinant XMAP215 to *Xenopus* egg extracts, which contains approximately 120 nM endogenous XMAP215 (ref. [26]). We expected the branched structures to appear larger due to longer and faster growing MTs, but less dense due to the unaltered level of MT nucleation[26]. We quantified the number of MTs by detecting all plus-tips over time as the readout for MT nucleation. Surprisingly, XMAP215 increased the number of MTs in a concentration-dependent manner (Supplementary Fig. 1a,b and Supplementary Video 1). The addition of 480 nM XMAP215 increased MT numbers up to

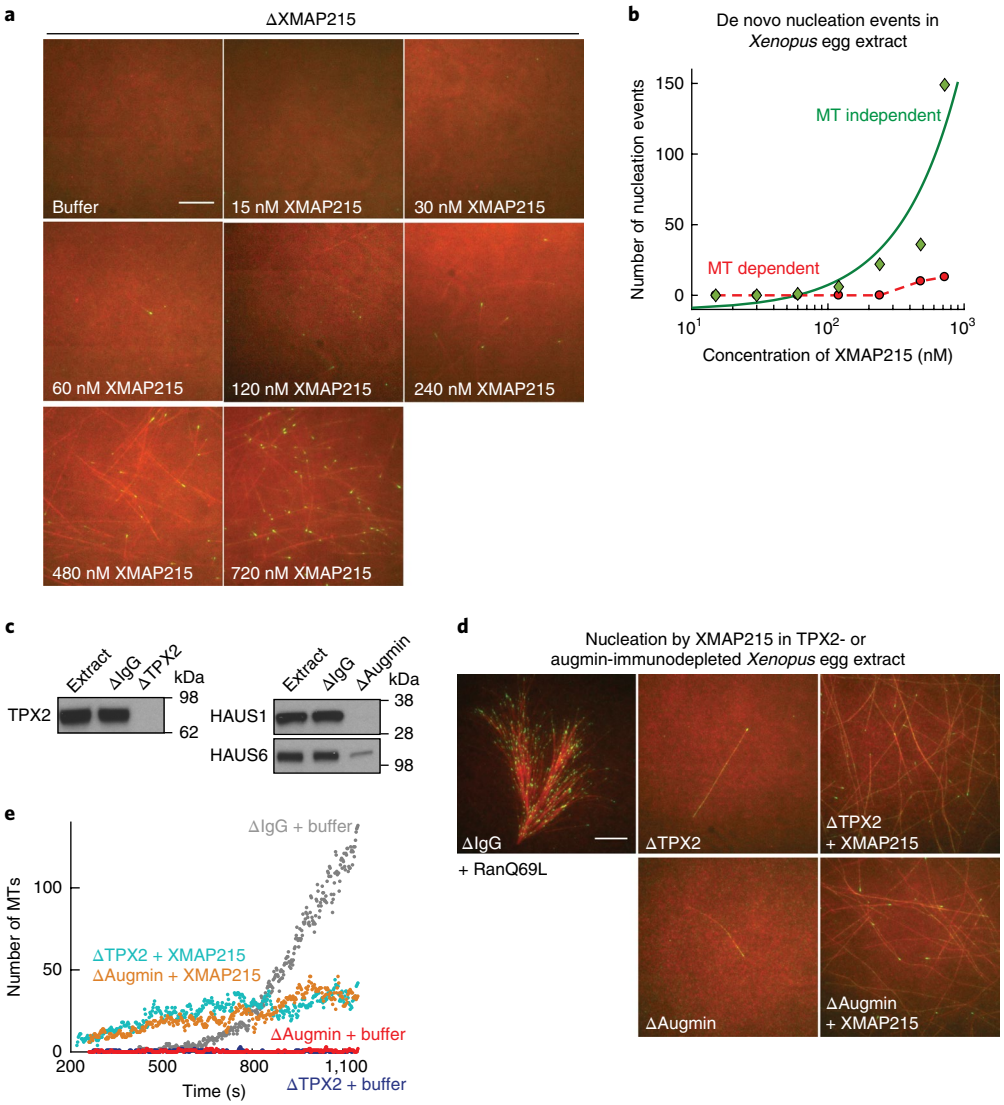

Fig. 2 | XMAP215 is required for all MT nucleation events. a, De novo (or MT-independent) nucleation events were observed with increasing XMAP215 concentration when XMAP215 was added back to XMAP215-depleted extracts without RanQ69L. Images are displayed at 700 seconds of the reaction. Scale bar, 10 µm. See Supplementary Fig. 2a,b and Supplementary Video 3. The experiment was repeated twice with independent extract preparations, along with more than three additional experiments, which were performed with fewer concentration points. **b**, Total number of MT-independent and MT-dependent nucleation events that occurred until 600 seconds of the reaction were counted and plotted against XMAP215 concentration. Data for MT-independent nucleation events versus XMAP215 concentration were fitted to a linear curve (solid green). XMAP215 concentration is plotted on a log scale. Few MT-dependent nucleation events were also observed (red circles). The analysis was repeated twice with independent extract preparations. See Supplementary Table 2 for source data. **c**, Immunoblot for TPX2 and augmin depletion corresponding to **d**,**e**. Augmin was immunodepleted using anti-HAUS1 antibodies and depletion was assessed by western blotting for two subunits: HAUS1 and HAUS6. **d**, XMAP215-GFP was added to TPX2 and augmin immunodepletion at 360 nM in addition to endogenous protein in the presence of 5.5 µM RanQ69L. Equal volume of buffer was added for control reactions. Representative images at 20 minutes are displayed. Scale bar, 10 µm. See Supplementary Video 4. **e**, EB1 comets in the entire field of view were tracked using the analysis procedure described in the Methods. The number of EB1 tracks were counted and plotted over time. The experiments in **c**–**e** were repeated twice with independent extract preparations, along with two supporting experiments. See Supplementary Fig. 9 for unprocessed blots.

30-fold, whereas the growth speed of MTs remained nearly constant (Supplementary Fig. 1b,c). These results show that XMAP215 has a dramatic effect on MT generation.

XMAP215 increases nucleation events, but is it required to generate MTs? To assess this, we immunodepleted XMAP215 from *Xenopus* extracts (Fig. 1a). Remarkably, MT nucleation was completely abolished in the absence of XMAP215 (Fig. 1b). This was confirmed by observing the reaction up to 1 hour, throughout the entire sample (2,000 fields of view) and across tens of extract preparations. This phenotype has previously been observed only by immunodepletion of γ-tubulin, the universal MT nucleator[36]. To verify the specificity of this effect, we added back purified XMAP215, which rescued the branched structures with comparable MT count to the control-depleted extracts (Fig. 1a,b and Supplementary Fig. 1d). Proteins such as transforming acidic coiled-coil-containing protein 3 (TACC3), α-tubulin, augmin, targeting protein for Xklp2 (TPX2) and γ-TuRC subunits were not depleted (Supplementary Fig. 1e). In summary, XMAP215 is required for the generation of MTs in *Xenopus* egg extracts.

Characterization of the MT nucleation activity of XMAP215. To further characterize its role, we investigated the effect of XMAP215

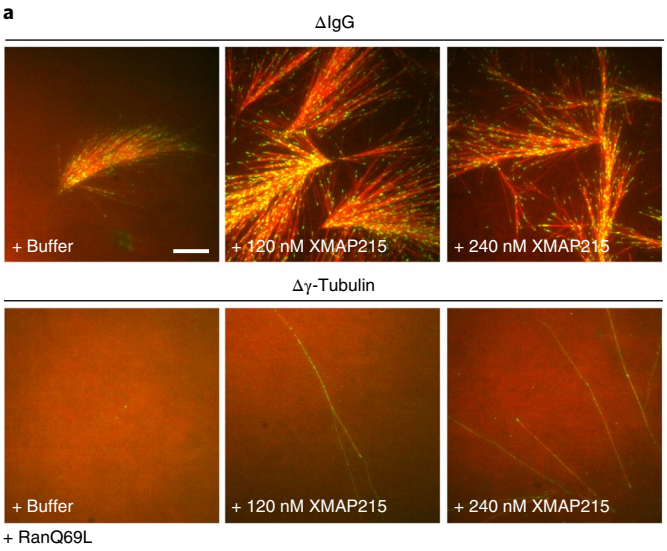

b

		+ XMAP215		
		0 nM	120 nM	240 nM
Number of MT-independent nucleations	ΔIgG	2	10	23
	Δγ-Tubulin	0	1	5
Number of MT-dependent nucleations	ΔIgG	178	1,872	1,892
	Δγ-Tubulin	0	1	3

Fig. 3 | γ-TuRC is required for MT nucleation by XMAP215. a, Branching MT nucleation was induced in control and γ-tubulin-depleted extracts with 5.5 μM RanQ69L. XMAP215-GFP was added at 120 nM and 240 nM concentrations in excess of the endogenous protein. Representative images are displayed at 1,100 seconds of the reaction. Scale bar, 10 μm. See Supplementary Video 5. The experiment was repeated with three independent extract preparations, including verification with the XenC antibody for γ-TuRC immunodepletion[5,11]. **b**, The number of MT-independent and MT-dependent nucleation events observed was tabulated with excess XMAP215 concentration. Nucleation events were counted until 800 seconds for each reaction. The few MTs that emerged in γ-tubulin-depleted extracts were counted manually (both MT-independent and MT-dependent nucleation events). For IgG depletion, the total number of MTs (EB1 comets) in the field of view was counted using image analysis, whereas de novo nucleation events were counted manually. The number of MT-dependent nucleation events was calculated by subtracting the MT-independent nucleation events from the total number of MTs. See Supplementary Fig. 3. The analyses were repeated twice with experiments performed on independent extract preparations, with one additional supporting set of results with anti-XenC immunodepletion.

concentration in MT nucleation and polymerization processes. We added increasing concentrations of XMAP215 to immunodepleted extracts and evaluated a range of XMAP215 concentrations: from sub-endogenous levels (15 nM) to sixfold the endogenous concentration (720 nM). No MTs formed at 15 nM XMAP215 and only a few MTs were visible at 30 nM (Fig. 1c,d and Supplementary Video 2). From 60 nM to 720 nM XMAP215, MT nucleation increased dramatically and the measured rate of MT nucleation varied linearly with XMAP215 concentration, without reaching saturation (Fig. 1e). We simultaneously measured the rate of polymerization or growth speed of MTs, which saturated at twice the endogenous concentration (240 nM), as previously reported[26].

In summary, MT nucleation and polymerization by XMAP215 demonstrates different characteristics. First, no saturation limit for MT nucleation was observed for the range of XMAP215 concentrations tested (Fig. 1e and Supplementary Fig. 1a,b), yet the MT polymerization rate saturated near the endogenous concentration (Fig. 1e and Supplementary Fig. 1c). Second, a minimum concentration of XMAP215 (30 nM) is required for nucleating MTs, whereas XMAP215 promotes MT growth even at low concentrations[24,26]. These results support that XMAP215 not only functions as a polymerase but also promotes MT nucleation in the cytoplasm.

XMAP215 is a general MT nucleation factor. These findings led us to investigate whether XMAP215 increases only branching MT nucleation events or generates MTs independently, which we define as de novo nucleation events. The number of de novo nucleation events and, consequently, the branched MT networks formed, increased linearly with XMAP215 concentration (Fig. 1f), suggesting that XMAP215 functions as a general MT nucleation factor. To directly characterize this, XMAP215-depleted extracts were used in the absence of RanQ69L, thereby not inducing branching MT nucleation, and increasing concentration of XMAP215 was added (Fig. 2a and Supplementary Video 3). Remarkably, de novo MT nucleation events increased by 150-fold between 60 nM and 720 nM XMAP215 (Fig. 2b). The occurrence of branching nucleation events was negligible (Fig. 2b). As before, no MTs formed at XMAP215 concentration ≤30 nM and the polymerization rate saturated at 240 nM (Supplementary Fig. 2a). In addition, we verified that XMAP215 stimulates de novo nucleation in the absence of the branching factors TPX2 and augmin[36] (Fig. 2c–e and Supplementary Video 4). Thus, XMAP215 functions as a general MT nucleation factor in the cytoplasm. Notably, MT nucleation by XMAP215 was indistinguishable in extracts depleted of TPX2 or augmin, excluding a specific synergy between TPX2 and XMAP215 in this assay that was previously observed in vitro[27].

To further understand the relationship between the nucleation and polymerization activities of XMAP215, we designed an experiment to specifically observe MT polymerization by XMAP215 in *Xenopus* extracts. Instead of observing endogenous MT nucleation, we added pre-formed MT seeds that were stabilized by GMPCPP to XMAP215-depleted extracts. Subsequently, wild-type XMAP215 was added back to initiate MT growth (Supplementary Fig. 2b–e). In the absence of XMAP215, polymerization was suppressed, resulting in infrequent EB1 blinking events on one end of MT seeds (roughly 20% seeds; Supplementary Fig. 2c,e). When 7.5 nM XMAP215 was added back, MT growth immediately occurred from a large proportion of seeds (nearly 70%). At 15 nM XMAP215, MTs polymerized from all seeds. By contrast, no MT nucleation events were observed in the absence of seeds at XMAP215 concentrations <30 nM (Figs. 1 and 2a,b). Thus, by titrating XMAP215 in *Xenopus* egg extracts, we found regimes where polymerization from the MT plus end occurs, whereas nucleation does not (Figs. 1 and 2a,b and Supplementary Fig. 2b–e), and where polymerization saturates, whereas nucleation continuously increases (Figs. 1c–f and 2a,b and Supplementary Fig. 1a–c).

γ-TuRC is required for MT nucleation by XMAP215. Our results show that XMAP215 is essential for MT generation, similar to the universal nucleator γ-TuRC, yet is γ-TuRC required for nucleation by XMAP215? To address this, we depleted the γ-TuRC from *Xenopus* extracts and induced MT nucleation by RanQ69L, whereas XMAP215 and proteins that are required for branching MT nucleation were not depleted (Supplementary Fig. 3a). Almost no MTs formed with endogenous levels of XMAP215 level in the absence of γ-TuRC (Fig. 3a). Surprisingly, both de novo and branching nucleation events were severely reduced even upon addition of excess XMAP215 to γ-TuRC-depleted extracts (Fig. 3a,b, Supplementary Fig. 3b,c and Supplementary Video 5). By specifically assaying

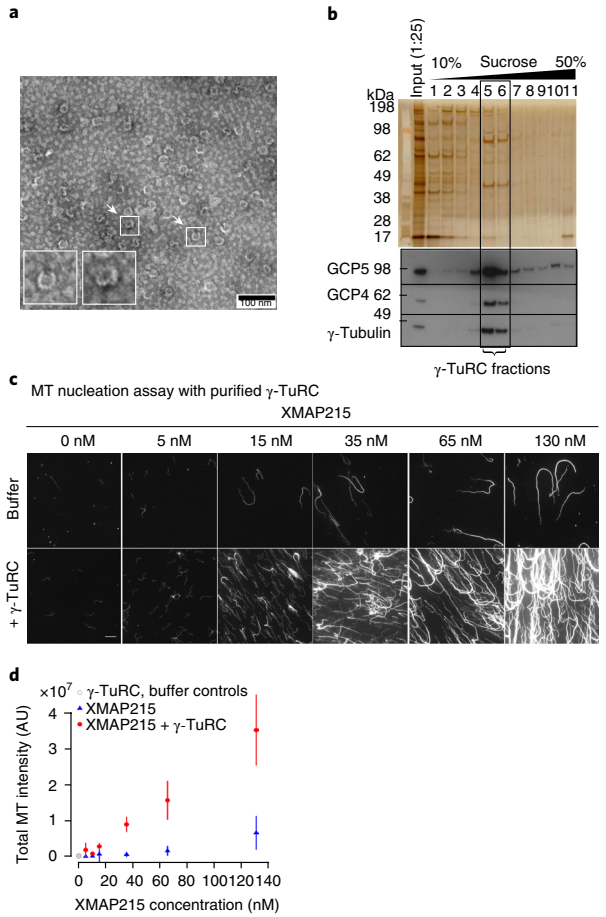

Fig. 4 | XMAP215 stimulates MT nucleation by γ-TuRC. a, Negative-stain electron microscopy shows 25-nm diameter ring structures (white arrows and insets) characteristic of γ-TuRC. Scale bar, 100 nm. The experiment was repeated three times, with at least three supporting experiments with sucrose gradient fractionated γ-TuRC, all showing distinct γ-TuRC ring structures. **b**, The peptide-eluted γ-TuRC was fractionated by sucrose gradient centrifugation. Fractions were analysed by silver-stained SDS-PAGE (top) and immunoblot (bottom) with antibodies against γ-tubulin, GCP5 and GCP4. These components were observed to peak in fractions 5 and 6, at the expected size for intact γ-TuRCs. The bands for GCP6, 5, 4, 3, 2, γ-tubulin, NEDD1 and Mzt2 can clearly be seen in fractions 5 and 6 using silver staining. A representative image is displayed and the experiment was repeated more than three times. See Supplementary Fig. 9 for unprocessed scans. **c**, The combination of the purified γ-TuRC and XMAP215 promotes MT nucleation in vitro. The purified γ-TuRC at 250–400 pM added to αβ-tubulin with GTP promotes MT nucleation compared to control (elution from IgG antibody-coated beads, upper left panel). The addition of recombinant XMAP215, at concentrations from 5 nM to 130 nM, promotes low levels of MT nucleation, with bundling and increased MT length seen at high concentrations. The addition of both XMAP215 and γ-TuRC together causes a significant increase in the number of MTs nucleated, greater than simply adding the MTs generated by each component independently. Representative fields of MTs are shown; nucleation assays were repeated with at least three independent γ-TuRC purifications. Scale bar, 10 μm. **d**, Fluorescent intensity was quantified as the readout of the amount of polymerized tubulin for ten fields of view for each reaction condition. Data from three independent γ-TuRC preparations were pooled and displayed as the mean ± s.d.; $n = 30$ fields of view analysed per reaction. The XMAP215 + γ-TuRC reactions had greater fluorescent intensity than control. A significant increase between MT mass can be seen starting from 35 nM XMAP215 when combined with γ-TuRC. See Supplementary Fig. 4. AU, arbitrary units.

de novo MT nucleation in *Xenopus* extracts as before (Fig. 2a), we further verified that XMAP215 promoted negligible de novo nucleation without γ-TuRC (Supplementary Fig. 3d,e). These results clearly demonstrate that both XMAP215 and γ-TuRC are required for all MT nucleation events in *Xenopus* extracts.

XMAP215 and γ-TuRC synergistically nucleate MTs in vitro. Because we found that XMAP215 and γ-TuRC are both required for nucleation in *Xenopus* extracts, we investigated their effect on MT nucleation in vitro. We first purified γ-TuRCs via affinity purification from *Xenopus* egg extracts. All components of γ-TuRC were present as confirmed by mass spectrometry (Supplementary Fig. 4a), whereas proteins such as XMAP215, TPX2, α-tubulin or TACC3 were not detected (Supplementary Fig. 4b). Furthermore, the characteristic ring shape of γ-TuRC was observed by electron microscopy (Fig. 4a). Affinity-purified γ-TuRCs were further purified by sucrose gradient centrifugation, where γ-TuRCs fractionated at the expected size (Fig. 4b).

MT nucleation was analysed in vitro by incubating soluble αβ-tubulin with purified γ-TuRCs and XMAP215 independently or together (Fig. 4b). At minimal αβ-tubulin concentration of 10–12 μM, γ-TuRC (250–400 pM) or XMAP215 alone nucleated few MTs above the buffer control. Addition of γ-TuRCs to increasing concentrations of XMAP215 (5–130 nM) resulted in a continuous increase in the amount of MTs observed (Fig. 4c). Remarkably, the low concentration of XMAP215 (5–30 nM) together with γ-TuRC resulted in 6–10-fold increase in the number of MTs generated when compared to the sum of MTs generated by XMAP215 and γ-TuRC individually (Supplementary Fig. 4c). With higher XMAP215 concentrations, even more prominent increase in MT generation was observed when the γ-TuRC was present (Fig. 4c). However, owing to the emergence of long, bundled MTs, individual MTs could not be counted and the total MT fluorescence intensity across all reactions was measured instead (Fig. 4d). These measurements demonstrate that XMAP215 and γ-TuRC together induce more MT generation than the sum of MT mass produced by either component individually across the range of XMAP215 concentration (Fig. 4c,d and Supplementary Fig. 4d). Similar results were obtained with the gradient-fractionated γ-TuRCs (Supplementary Fig. 4e). This in vitro reconstitution agrees with our results in *Xenopus* extracts (Figs. 1 and 2). Thus, XMAP215 and γ-TuRC synergistically promote MT nucleation both in vitro and ex vivo.

TOG domains of XMAP215 are essential for MT nucleation. We next asked what regions of XMAP215 are required for MT nucleation activity in the cytoplasm. We generated versions of XMAP215 lacking TOG domains from the N terminus or missing its C terminus. All constructs were tested for their nucleation activity in *Xenopus* extracts following the depletion of endogenous XMAP215. Branching MT nucleation was stimulated by the C-terminal half of TPX2 in addition to RanQ69L as described previously[36], which allows for robust measurements of low nucleation levels by some XMAP215 constructs.

Deleting the TOG1 domain (TOG2-CT) caused significant reduction in MT nucleation (Fig. 5a, Supplementary Fig. 5a,b and Supplementary Video 6), and further deletion of TOG2 (TOG3-CT) or TOG1–4 domains (TOG5-CT) completely abrogated MT generation. Smaller branched structures were generated when the C-terminal domain of XMAP215 was removed (TOG1-5), whereas further truncation from the C terminus preserving TOG1–4 regions also reduced the nucleation activity of the protein (Fig. 5b,c and Supplementary Video 7). These results indicate that the entire protein is needed for full MT nucleation activity, with the TOG domains being essential for retaining a minimal level of nucleation.

The TOG1 and TOG2 domains of XMAP215 linked to a MT-binding region have been reported to recapitulate the minimal

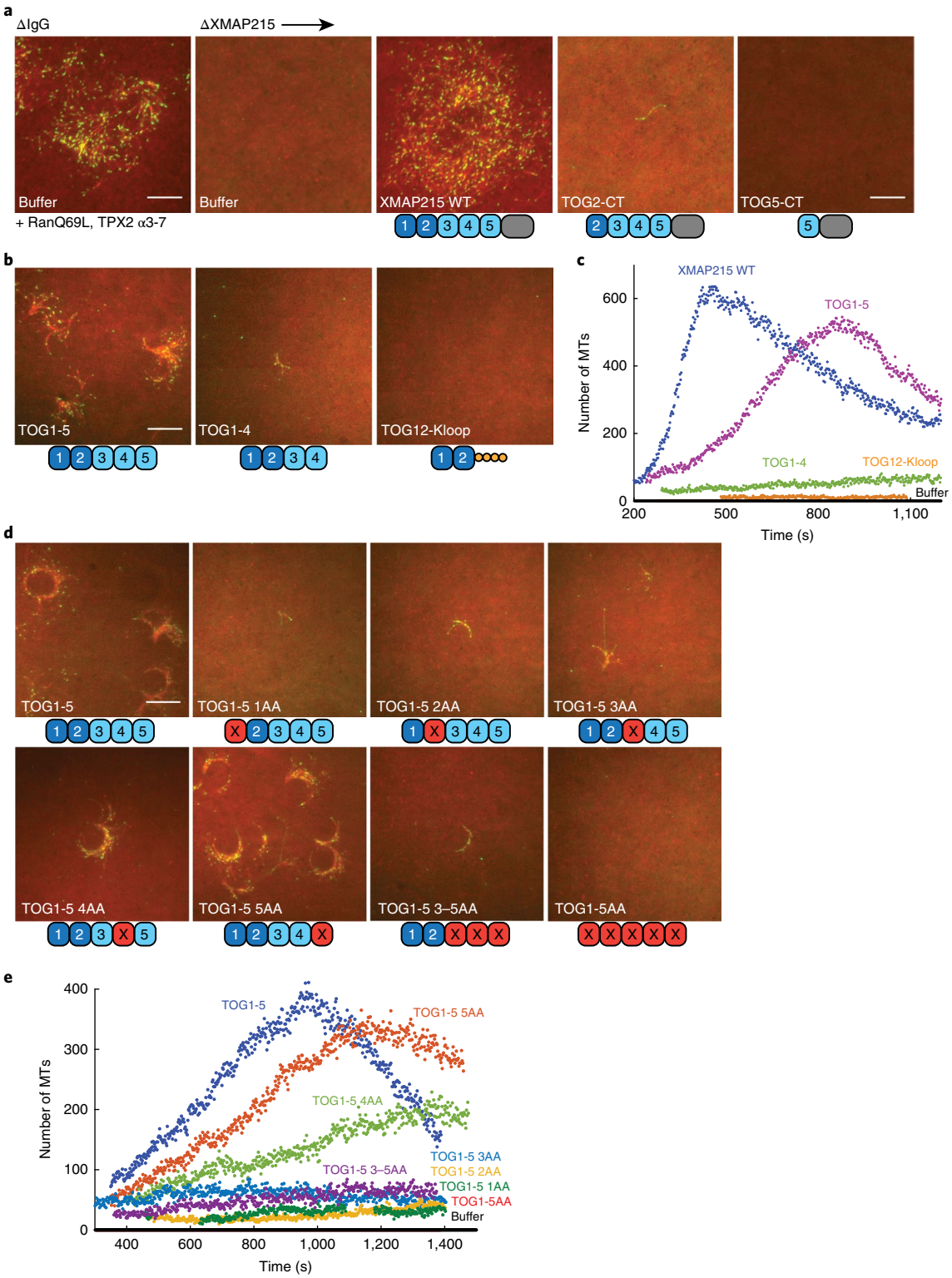

Fig. 5 | MT nucleation by XMAP215 protein constructs in *Xenopus* egg extracts. Branching MT nucleation activity of XMAP215 constructs. All proteins were added back to the XMAP215-depleted extracts at a final concentration of 120 nM in the presence of 5.5 μM RanQ69L and 1 μM GST-TPX2 α3-7. All experiments and analyses were repeated with at least three independent extract preparations. **a**, Representative images are displayed for N-terminal deletion constructs at 560 seconds of the reaction. Scale bar, 10 μm. See Supplementary Fig. 5a,b and Supplementary Video 6. **b**, Representative images are displayed for C-terminal deletion constructs at 480 seconds of the reaction. Scale bar, 10 μm. See Supplementary Video 7. **c**, The number of EB1 comets was detected, counted and plotted with time for protein constructs displayed in **b**. **d**, Branching MT nucleation activity of tubulin-binding mutant constructs of the TOG1-5 protein. Representative images are displayed at 650 seconds of the reaction. Scale bar, 10 μm. See Supplementary Video 8. AA, amino acid. **e**, The number of EB1 comets was detected, counted and plotted with time for the protein constructs displayed in **d**. See Supplementary Fig. 5.

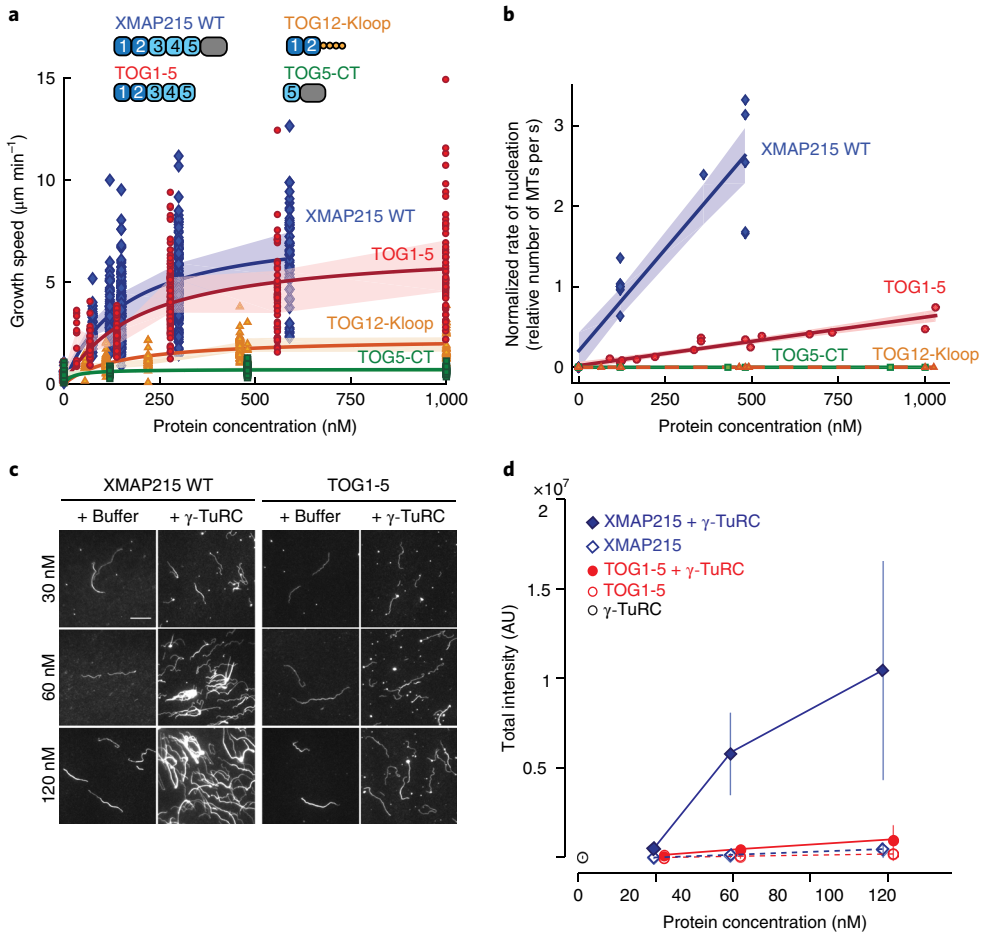

Fig. 6 | The C terminus of XMAP215 is required for MT nucleation with γ-TuRC. **a**, Polymerization from stabilized seeds was performed with several XMAP215 constructs: wild-type XMAP215, TOG1-5, TOG12-Kloop and TOG5-CT. Growth speed was measured from kymographs and plotted against the protein concentration. The number of kymographs analysed: buffer ($n=21$); XMAP215 WT: 75 nM ($n=43$), 120 nM ($n=62$), 150 nM ($n=141$), 300 nM ($n=131$), 590 nM ($n=53$); TOG1-5: 35 nM ($n=12$), 70 nM ($n=24$), 140 nM ($n=57$), 280 nM ($n=84$), 560 nM ($n=49$), 1,000 nM ($n=59$); TOG12-Kloop: 55 nM ($n=21$), 110 nM ($n=51$), 220 nM ($n=44$), 460 nM ($n=70$), 1,000 nM ($n=32$); TOG5-CT: 120 nM ($n=53$), 480 nM ($n=74$), 1,000 nM ($n=46$). The shaded region represents the s.d. at individual concentrations. Michaelis–Menten fit to all measurements versus concentration is displayed (solid curves). **b**, Branching MT nucleation activity of XMAP215 constructs in **a** was observed in *Xenopus* egg extracts. Proteins were added to the XMAP215-depleted extracts at a specified final concentration along with 5.5 μM RanQ69L and 1 μM GST-TPX2 α3-7. The rate of MT nucleation was measured from the linear region of the nucleation curves (the representative plot for TOG1-5 is shown in Supplementary Fig. 6b). The rate of nucleation by 120 nM wild-type XMAP215 was normalized to 1 in each experimental set with *Xenopus* extracts. Where more than one reaction at 120 nM wild-type XMAP215 was performed, their average was set to 1. Data were pooled from the following independent extract preparations: wild-type XMAP215 (8), TOG1-5 protein (4), TOG12-Kloop (3) and TOG5-CT (2). Normalized rate of nucleation versus protein concentration was fit to a straight line, with the shaded region representing the 95% confidence interval. See Supplementary Video 9. **c**,**d**, Purified γ-TuRCs were incubated with wild-type XMAP215 or TOG1-5 to promote MT nucleation in vitro. The addition of 30–120 nM wild-type XMAP215 promotes synergistic MT nucleation with γ-TuRC, whereas TOG1-5 shows minimal synergy with γ-TuRC. Representative fields of MTs are displayed. Experiments were repeated with two independent γ-TuRC purifications. Scale bar, 10 μm. Quantification of the total fluorescent intensity are also shown (**d**). All data from two independent γ-TuRC preparations were pooled and plotted as the mean ± s.d., except the 30 nM TOG1-5 condition, which was performed with one γ-TuRC preparation. γ-TuRC ($n=44$); XMAP215: 30 nM ($n=20$), 60 nM ($n=50$), 120 nM ($n=43$); TOG1-5: 30 nM ($n=20$), 60 nM ($n=39$), 120 nM ($n=44$); γ-TuRC + XMAP215 30 nM ($n=20$), 60 nM ($n=45$), 120 nM ($n=39$); γ-TuRC + TOG1-5: 30 nM ($n=20$), 60 nM ($n=41$), 120 nM ($n=41$). *n* represents the number of fields of view analysed. See Supplementary Table 1 for source data of Fig. 6b–d and Supplementary Fig. 6.

polymerase activity[24]. This protein construct (TOG12-Kloop) did not have any discernable nucleation activity, suggesting that the minimal polymerization domains are not sufficient to promote MT nucleation.

Because TOG domains interact with αβ-tubulin to promote polymerization[30], we tested whether disrupting αβ-tubulin binding to TOGs by mutating two residues in each TOG domain[24] affects the nucleation activity of XMAP215. This mutation in all TOGs within the full-length XMAP215 and the TOG1-5 construct completely abolished MT nucleation activity (Fig. 5d,e, Supplementary Fig. 5c,d and Supplementary Video 8). Mutating residues in TOG domains 1–3 individually dramatically reduced the nucleation activity of TOG1-5, with the more N-terminally situated TOGs having a greater effect, matching their described function in polymerization[24]. By contrast, mutation of TOG4 had a minor effect, whereas mutating TOG5 did not significantly impair MT nucleation. Interestingly, the loss of the TOG5 domain caused significant reduction in MT nucleation (Fig. 5b,c; compare TOG1-5 with TOG1-4), whereas mutating TOG5 did not, suggesting that the role of TOG5 may not involve its interaction with αβ-tubulin dimers.

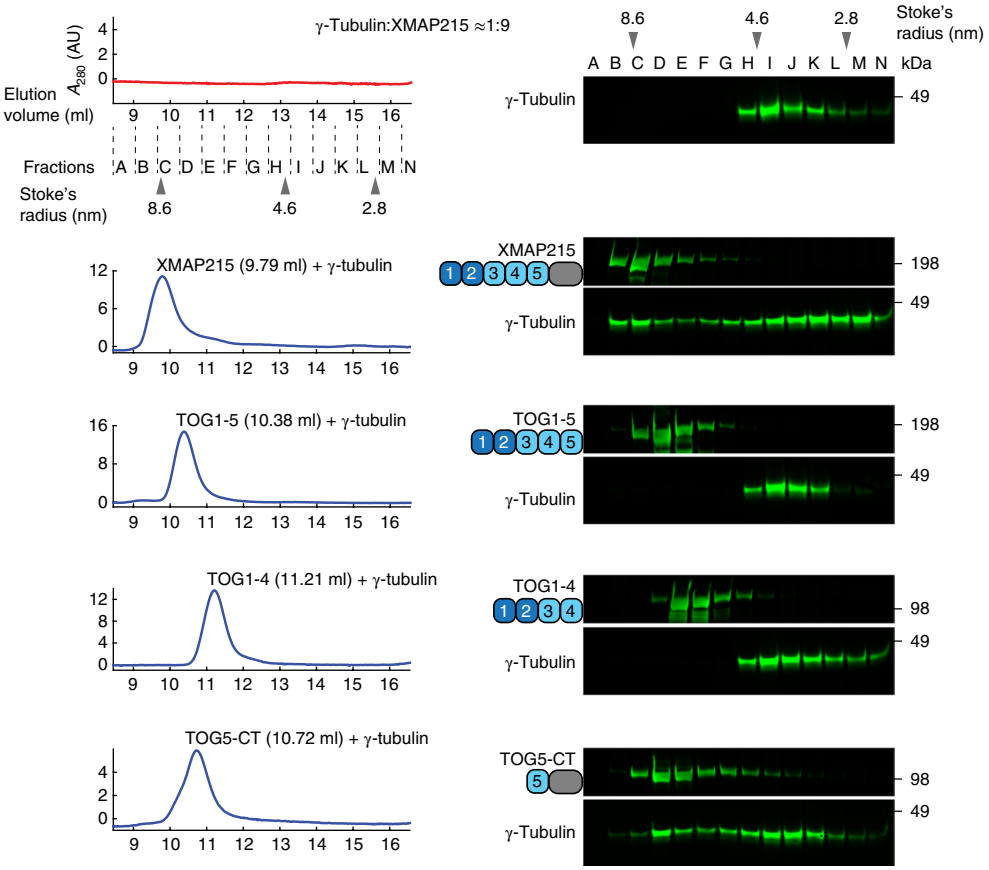

Fig. 7 | XMAP215 interacts with γ-tubulin via its C-terminal domains. Size-exclusion chromatography was performed with 140 nM human γ-tubulin alone and with 1–1.4 μM XMAP215 protein constructs. A sample volume of 500 μl was injected into the column, and 300 μl fractions were collected. Alternate fractions eluted between 8.5 ml and 16.6 ml were analysed via SDS–PAGE followed by immunoblot with γ-tubulin antibodies and GFP antibodies to detect the elution profile of γ-tubulin and GFP-labelled XMAP215 proteins, respectively. To assess the XMAP215 region that γ-tubulin interacts with, a shift in the γ-tubulin signal was observed. Stoke's radii of reference proteins are marked at their peak elution: thyroglobulin (8.6 nm), aldolase (4.6 nm) and ovalbumin (2.8 nm). The contrast of each image was adjusted to display the entire elution profile clearly. Each chromatography run was repeated at least twice on different days at the specified concentration, and at least one additional supporting experiment for each displayed run (more than nine supporting runs in total) was performed at slightly different protein concentrations. The void volume of the column was measured as 8.7–8.8 ml. See Supplementary Fig. 8a–c. See also Supplementary Fig. 9 for unprocessed scans. A_{280}, absorbance at 280 nm. AU, arbitrary units.

Finally, maintaining the αβ-tubulin binding of TOG1 and TOG2 (TOG1-5 3–5AA, Fig. 5d) did not restore nucleation, demonstrating that TOG1 and TOG2 alone are not able to promote MT nucleation. Taken together, the interaction between αβ-tubulin and the TOG domains of XMAP215, in particular, by the N-terminally situated TOGs, is important for MT nucleation activity.

The C terminus of XMAP215 is required for efficient MT nucleation. To compare how the domains of XMAP215 contribute to MT polymerization versus MT nucleation, we chose three constructs: the N-terminal TOG1–5 domains (TOG1-5), the construct containing TOG5 and the C terminus (TOG5-CT) and the minimal polymerase (TOG12-Kloop). First, we performed in vitro MT polymerization from stabilized MT seeds in the presence of these constructs. Wild-type XMAP215 promoted MT plus-end growth in a concentration-dependent manner (Fig. 6a and Supplementary Fig. 6a), as described previously[23,24,26,37]. TOG1-5 strongly promoted MT polymerization to an extent similar to the full-length protein. The maximum MT polymerization rate by the minimal polymerase TOG12-Kloop was 2–3-fold lower than wild-type XMAP215, as previously reported[24]. Most importantly, the C-terminal construct TOG5-CT did not increase the MT polymerization rate even at high protein concentrations. In summary, the N-terminal TOG domains of XMAP215 constitute the MT-polymerizing region of the protein and its C terminus is neither required for nor affects the growth rate of MT plus ends.

To thoroughly compare the nucleation activity to polymerization by these domains, we repeated the branching MT nucleation assay in *Xenopus* extracts as a function of XMAP215 concentration. As before, upon depletion of endogenous XMAP215 followed by add-back of increasing concentrations of wild-type XMAP215, an increase in the rate of MT nucleation was observed (Fig. 6b, Supplementary Fig. 6b and Supplementary Video 9). Although add-back of TOG1-5 forms MT networks, the rate of MT nucleation was significantly reduced. Even at high TOG1-5 concentrations (500 nM to 1 μM), the rate of MT nucleation remained lower than at endogenous concentrations of full-length XMAP215 (120 nM). Neither the addition of up to 1 μM of the C-terminal construct (TOG5-CT) nor the minimal polymerase (TOG12-Kloop) restored MT nucleation. The side-by-side comparison of these constructs in MT polymerization and nucleation assays (Fig. 6a,b) demonstrates that the C terminus of XMAP215 does not directly promote polymerization, yet is required for rapid MT nucleation in *Xenopus* extracts.

To further analyse the requirement of the C-terminus of XMAP215 in nucleating MTs, we performed in vitro MT nucleation assay with purified γ-TuRC and increasing concentrations

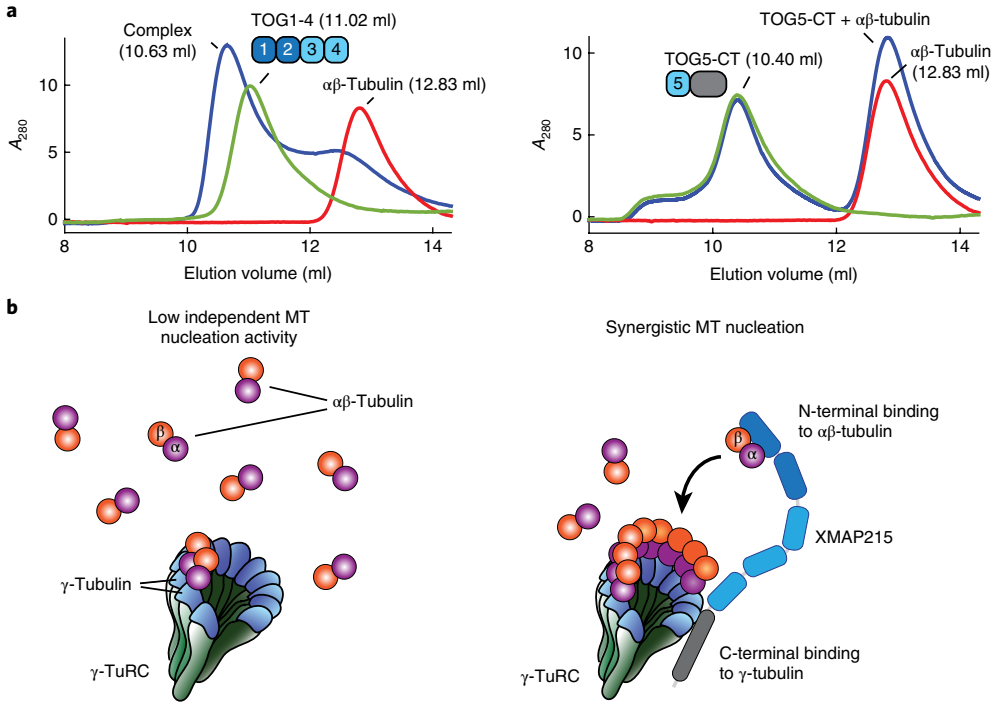

Fig. 8 | The N terminus of XMAP215 interacts with αβ-tubulin, and a model for how XMAP215 and γ-TuRC promote MT nucleation. a, The XMAP215 N-terminal TOG1-4 construct or the C-terminal TOG5-CT construct (5–6 μM) and bovine αβ-tubulin (6.2 μM) were mixed and applied to size-exclusion chromatography. A sample volume of 100 μl was injected into the column. Each chromatography run was performed once at the specified concentration. More than three additional supporting experiments were performed either with slightly different protein concentrations or using alternative protein constructs. The void volume of the column was measured as 8.7–8.8 ml. See Supplementary Fig. 8d. See also Supplementary Fig. 9 for unprocessed scans. **b**, Schematic representation for how XMAP215 and γ-TuRC could together promote MT nucleation. Although γ-TuRC independently induces low MT nucleation, its cooperation with XMAP215 promotes efficient nucleation of MTs. The synergistic MT nucleation model proposes that XMAP215 binds to the γ-TuRC with its C terminus and promotes the assembly of αβ-tubulin dimers onto the γ-TuRC via its N terminus.

of TOG1-5 protein (Fig. 6c). Similar to full-length XMAP215, TOG1-5 alone displays low nucleation activity. Combining γ-TuRC and TOG1-5 resulted in slightly increased MT nucleation compared to γ-TuRC alone (Fig. 6c, Supplementary Fig. 6c), yet TOG1-5 induced lower MT nucleation with γ-TuRC than the wild-type XMAP215. At higher protein concentrations, the difference in nucleation activity of full-length XMAP215 and TOG1-5 was more pronounced and TOG1-5 shows a markedly reduced effect on MT generation when combined with γ-TuRC (Fig. 6d). Together, these results demonstrate that the polymerizing region of XMAP215, the N-terminal TOG1-5, is not sufficient to promote MT nucleation similar to the full-length XMAP215 and γ-TuRC, and that the conserved C-terminus is required for robust MT nucleation.

XMAP215 and γ-TuRC components interact in the *Xenopus* egg extracts. Because γ-TuRC and XMAP215 cooperate to generate MTs, we hypothesized that these components may interact in *Xenopus* egg extracts. Indeed, components of γ-TuRC co-immunoprecipitate with XMAP215 (Supplementary Fig. 7a) and, reciprocally, endogenous XMAP215 was co-precipitated with γ-TuRC (Supplementary Fig. 7b), confirming an interaction between these components in egg extracts. Notably, the branching factor TPX2 did not co-precipitate in either experiment, whereas augmin did not co-precipitate with XMAP215, verifying the specificity of this interaction. We note that in *Drosophila* S2 cells, XMAP215 and augmin were co-immunoprecipitated[38]. This could be owing to system-specific differences, such as the species, cell cycle state or the presence of MTOCs that are absent from *Xenopus* extracts.

It is noteworthy that αβ-tubulin was not co-immunoprecipitated with endogenous XMAP215 (Supplementary Fig. 7a). This was surprising because XMAP215 and αβ-tubulin directly interact in vitro[23,24]. We determined that XMAP215 and αβ-tubulin interact in vitro using size-exclusion chromatography only under low-salt buffer[23,24] (75 mM NaCl; Supplementary Fig. 7c). This interaction was not maintained near the physiological salt concentration (150 mM NaCl), suggesting that the binding of XMAP215 to αβ-tubulin is transient in the cytoplasmic environment of *Xenopus* extracts.

The C terminus of XMAP215 directly binds to γ-tubulin. To further characterize the interaction between XMAP215 and γ-TuRC, we specifically tested binding between XMAP215 and γ-tubulin, the most abundant component of the γ-TuRC. We performed size-exclusion chromatography with purified human γ-tubulin and XMAP215. To prevent the formation of γ-tubulin filaments at several hundred nanomolar concentration[39], we used a low-molar ratio of γ-tubulin to XMAP215. In this setup, γ-tubulin alone elutes in fractions H–K (Fig. 7) and partially oligomerizes in the chromatography buffer (compare to Supplementary Fig. 8a). Interestingly, in the presence of XMAP215, γ-tubulin shifts towards an earlier elution volume corresponding to the elution of XMAP215, demonstrating its direct interaction with γ-tubulin. This binding was verified using in vitro immunoprecipitations (Supplementary Fig. 8b). Notably, this interaction occurs even at the low γ-tubulin concentrations used in these experiments (140 nM in Fig. 7 and 80 nM in Supplementary Fig. 8b), which are within the cytoplasmic γ-tubulin concentrations[40]. Mutating the residues that are essential for αβ-tubulin interaction in TOG domains did not abolish γ-tubulin binding (Supplementary Fig. 8c). Next, we identified the XMAP215 domain responsible for interacting with γ-tubulin. The N-terminal constructs containing TOG1–4 or TOG1–5, or the

protein containing TOG1 and TOG2 repeated twice did not interact with γ-tubulin (Fig. 7 and Supplementary Fig. 8C). Surprisingly, the C-terminal construct containing TOG5 and the C-terminal domain (TOG5-CT) strongly shifted γ-tubulin to an earlier elution volume, similar to the full-length XMAP215 (Fig. 7). These results demonstrate that XMAP215 directly binds to γ-tubulin, potentially in an oligomeric form, via its C-terminal domain.

We next validated the region of XMAP215 that interacts with αβ-tubulin using size-exclusion chromatography. The N-terminal TOG1-4 protein formed a complex with αβ-tubulin similar to wild-type XMAP215, whereas the C-terminal construct TOG5-CT did not bind to αβ-tubulin (Fig. 8a and Supplementary Fig. 8d). Taken together, these results show that the N terminus of XMAP215 binds to αβ-tubulin, whereas its C terminus interacts with γ-tubulin.

Discussion

How MT nucleation occurs is critical for understanding how MT cytoskeletal structures that enable cell function are assembled. γ-TuRC has been thought to have a prominent role in MT nucleation since its discovery in 1989 (ref. [41]), but evidence has suggested that other factors might also exist. In this study, we uncover that the major polymerase of the cell, XMAP215, is a principal MT nucleation factor that directly interacts with γ-tubulin and functions synergistically with γ-TuRC to generate MTs in the cytoplasm.

We propose several reasons why the role of XMAP215 in MT nucleation has been underappreciated until now. Of primary importance, assays to resolve MT nucleation in the cytoplasm and to distinguish it from plus-end growth were previously unavailable. In addition, compensatory nucleation mechanisms in the mitotic spindle[11,26,42], introduction of MTOCs such as centrosomes[32] that contain XMAP215 (ref. [43]) or incomplete loss of XMAP215 (refs [20,44]) could have masked its function in MT nucleation. Here, by developing a high-resolution assay and analyses system, stimulating nucleation without MTOCs, and through complete XMAP215 depletion, we demonstrate that XMAP215, along with γ-TuRC, is necessary for all nucleation events in *Xenopus* egg extracts and determines the rate of MT generation in the cytoplasm.

One widely accepted model for MT nucleation[7] proposes that γ-tubulin complexes perform the entire nucleation process. In this scenario, XMAP215, acting solely as a polymerase, catalyses the addition of αβ-tubulin dimers to the plus end after MT nucleation has occurred[26]. By contrast, our study clearly demonstrates that XMAP215 and γ-TuRC function cooperatively in the nucleation process, whereas either factor independently supports low MT nucleation (Fig. 8b, left). What is the molecular mechanism by which γ-TuRC and XMAP215 nucleate MTs? We propose a synergistic nucleation model in which both XMAP215 and the γ-TuRC are directly involved in assembling MT precursors. The C-terminal region of XMAP215 binds to the γ-TuRC where the TOG domains recruit αβ-tubulin dimers and both factors together form the MT nucleation intermediates (Fig. 8b, right). The domain organization of the conserved C terminus still remains to be characterized, but the existence of a sixth TOG domain has been speculated[45,46], which could be a potential γ-tubulin interaction site. In the N terminus, TOG1 and TOG2 domains could primarily recruit αβ-tubulin dimers, whereas the later TOG domains stabilize the newly forming MT. This is supported by recent work proposing the interaction of TOG5 with lattice-incorporated αβ-tubulin[31,47]. Following MT nucleation, XMAP215 could translate with the growing MT plus end to catalyse MT polymerization. In the future, it will be important to further investigate the mechanism of how XMAP215 and γ-TuRC cooperate to nucleate a MT using single-molecule techniques and structural studies.

Because MT nucleation is the rate-limiting process in constructing the cytoskeleton, the activity of the principal nucleation module consisting of XMAP215 and γ-TuRC must be critically regulated in space and time to rapidly assemble complex MT structures. Although γ-TuRC has been proposed to be regulated by activator proteins such as cyclin-dependent kinase 5 (CDK5) regulatory subunit-associated protein 2 (CDK5RAP2)[15], it is feasible that XMAP215 is also regulated. For example, the localization of XMAP215 at the centrosome by TACC3 (ref. [48]) could function to concentrate XMAP215 near γ-TuRCs, or post-translational modifications[19,49] could temporally regulate its nucleation activity. With the discovery of the cooperation between XMAP215 and γ-TuRC in the MT nucleation process, we can now begin evaluating additional factors that regulate MT generation.

Methods

Methods, including statements of data availability and any associated accession codes and references, are available at https://doi.org/10.1038/s41556-018-0091-6.

Received: 16 November 2017; Accepted: 20 March 2018;
Published online: 25 April 2018

References

1. Voter, W. A. & Erickson, H. P. The kinetics of microtubule assembly. Evidence for a two-stage nucleation mechanism. *J. Biol. Chem.* **259**, 10430–10438 (1984).
2. Petry, S. & Vale, R. Microtubule nucleation at the centrosome and beyond. *Nat. Cell Biol.* **17**, 1089–1093 (2015).
3. Luders, J. & Stearns, T. Microtubule-organizing centres: a re-evaluation. *Nat. Rev. Mol. Cell Biol.* **8**, 161–167 (2007).
4. Wiese, C. & Zheng, Y. Microtubule nucleation: γ-tubulin and beyond. *J. Cell Sci.* **119**, 4143–4153 (2006).
5. Zheng, Y., Wong, M. L., Alberts, B. & Mitchison, T. Nucleation of microtubule assembly by a γ-tubulin-containing ring complex. *Nature* **378**, 578–583 (1995).
6. Moritz, M., Braunfeld, M. B., Sedat, J. W., Alberts, B. & Agard, D. A. Microtubule nucleation by γ-tubulin-containing rings in the centrosome. *Nature* **378**, 638–640 (1995).
7. Kollman, J. M., Merdes, A., Mourey, L. & Agard, D. A. Microtubule nucleation by γ-tubulin complexes. *Nat. Rev. Mol. Cell Biol.* **12**, 709–721 (2011).
8. Moritz, M., Braunfeld, M. B., Guénebaut, V., Heuser, J. & Agard, D. A. Structure of the γ-tubulin ring complex: a template for microtubule nucleation. *Nat. Cell Biol.* **2**, 365–370 (2000).
9. Kollman, J. M., Polka, J. K., Zelter, A., Davis, T. N. & Agard, D. A. Microtubule nucleating γ-TuSC assembles structures with 13-fold microtubule-like symmetry. *Nature* **466**, 879–882 (2010).
10. Caudron, N. Microtubule nucleation from stable tubulin oligomers. *J. Biol. Chem.* **277**, 50973–50979 (2002).
11. Groen, A. C., Maresca, T. J., Gatlin, J. C., Salmon, E. D. & Mitchison, T. J. Functional overlap of microtubule assembly factors in chromatin-promoted spindle assembly. *Mol. Biol. Cell* **20**, 2766–2773 (2009).
12. Hannak, E. et al. The kinetically dominant assembly pathway for centrosomal asters in *Caenorhabditis elegans* is γ-tubulin dependent. *J. Cell Biol.* **157**, 591–602 (2002).
13. Rogers, G. C., Rusan, N., Peifer, M. & Rogers, S. L. A multicomponent assembly pathway contributes to the formation of acentrosomal microtubule arrays in interphase *Drosophila* cells. *Mol. Biol. Cell* **19**, 3163–3178 (2008).
14. Moritz, M., Zheng, Y., Alberts, B. M. & Oegema, K. Recruitment of the γ-tubulin ring complex to *Drosophila* salt-stripped centrosome scaffolds. *J. Cell Biol.* **142**, 775–786 (1998).
15. Choi, Y., Liu, P., Sze, S., Dai, C. & Qi, R. CDK5RAP2 stimulates microtubule nucleation by the γ-tubulin ring complex. *J. Cell Biol.* **191**, 1089–1095 (2010).
16. Liu, P., Choi, Y. & Qi, R. NME7 is a functional component of the γ-tubulin ring complex. *Mol. Biol. Cell* **25**, 2017–2025 (2014).
17. Oegema, K. et al. Characterization of two related *Drosophila* γ-tubulin complexes that differ in their ability to nucleate microtubules. *J. Cell Biol.* **144**, 721–733 (1999).
18. Kollman, J. M. et al. Ring closure activates yeast γTuRC for species-specific microtubule nucleation. *Nat. Struct. Mol. Biol.* **22**, 132–137 (2015).
19. Gard, D. L. & Kirschner, M. W. A microtubule-associated protein from *Xenopus* eggs that specifically promotes assembly at the plus-end. *J. Cell Biol.* **105**, 2203–2215 (1987).
20. Tournebize, R. et al. Control of microtubule dynamics by the antagonistic activities of XMAP215 and XKCM1 in *Xenopus* egg extracts. *Nat. Cell Biol.* **2**, 13–19 (2000).
21. Popov, A. V. et al. XMAP215 regulates microtubule dynamics through two distinct domains. *EMBO J.* **20**, 397–410 (2001).

22. Al-Bassam, J., Van Breugel, M., Harrison, S. C. & Hyman, A. Stu2p binds tubulin and undergoes an open-to-closed conformational change. *J. Cell Biol.* **172**, 1009–1022 (2006).
23. Brouhard, G. J. et al. XMAP215 is a processive microtubule polymerase. *Cell* **132**, 79–88 (2008).
24. Widlund, P. O. et al. XMAP215 polymerase activity is built by combining multiple tubulin-binding TOG domains and a basic lattice-binding region. *Proc. Natl Acad. Sci. USA* **108**, 2741–2746 (2011).
25. Al-Bassam, J. et al. Fission yeast Alp14 is a dose-dependent plus end-tracking microtubule polymerase. *Mol. Biol. Cell* **23**, 2878–2890 (2012).
26. Reber, S. B. et al. XMAP215 activity sets spindle length by controlling the total mass of spindle microtubules. *Nat. Cell Biol.* **15**, 1116–1122 (2013).
27. Roostalu, J., Cade, N. & Surrey, T. Complementary activities of TPX2 and chTOG constitute an efficient importin-regulated microtubule nucleation module. *Nat. Cell Biol.* **17**, 1422–1434 (2015).
28. Wilde, A. & Zheng, Y. Stimulation of microtubule aster formation and spindle assembly by the small GTPase Ran. *Science* **284**, 1359–1362 (1999).
29. Slep, K. & Vale, R. Structural basis of microtubule plus end tracking by XMAP215, CLIP-170, and EB1. *Mol. Cell* **27**, 976–991 (2007).
30. Ayaz, P., Ye, X., Huddleston, P., Brautigam, C. A. & Rice, L. M. A TOG:αβ -tubulin complex structure reveals conformation-based mechanisms for a microtubule polymerase. *Science* **337**, 857–860 (2012).
31. Byrnes, A. E. & Slep, K. C. TOG-tubulin binding specificity promotes microtubule dynamics and mitotic spindle formation. *J. Cell Biol.* **216**, 1641–1657 (2017).
32. Popov, A. V., Severin, F. & Karsenti, E. XMAP215 is required for the microtubule-nucleating activity of centrosomes. *Curr. Biol.* **12**, 1326–1330 (2002).
33. Wieczorek, M., Bechstedt, S., Chaaban, S. & Brouhard, G. J. Microtubule-associated proteins control the kinetics of microtubule nucleation. *Nat. Cell Biol.* **17**, 907–916 (2015).
34. Ohi, R. & Zanic, M. Ahead of the curve: new insights into microtubule dynamics. *F1000Res.* **5**, 314 (2016).
35. Roostalu, J. & Surrey, T. Microtubule nucleation: beyond the template. *Nat. Rev. Mol. Cell Biol.* **18**, 702–710 (2017).
36. Petry, S., Groen, A., Ishihara, K., Mitchison, T. & Vale, R. Branching microtubule nucleation in *Xenopus* egg extracts mediated by augmin and TPX2. *Cell* **152**, 768–777 (2013).
37. Zanic, M., Widlund, P. O., Hyman, A. A. & Howard, J. Synergy between XMAP215 and EB1 increases microtubule growth rates to physiological levels. *Nat. Cell Biol.* **15**, 688–693 (2013).
38. Bucciarelli, E. et al. *Drosophila* Dgt6 interacts with Ndc80, Msps/XMAP215, and γ-tubulin to promote kinetochore-driven MT formation. *Curr. Biol.* **19**, 1839–1845 (2009).
39. Moritz, M., Rice, L. M. & Agard, D. A. *Microtubule Nucleation* (Wiley-VCH, Weinheim, 2004).
40. Wuhr, M. et al. Deep proteomics of the *Xenopus laevis* egg using an mRNA-derived reference database. *Curr. Biol.* **24**, 1467–1475 (2014).
41. Oakley, C. E. & Oakley, B. R. Identification of γ-tubulin, a new member of the tubulin superfamily encoded by *mipA* gene of *Aspergillus nidulans*. *Nature* **338**, 662–664 (1989).
42. Srayko, M., Kaya, A., Stamford, J. & Hyman, A. A. Identification and characterization of factors required for microtubule growth and nucleation in the early *C. elegans* embryo. *Dev. Cell* **9**, 223–236 (2005).
43. Andersen, J. S. et al. Proteomic characterization of the human centrosome by protein correlation profiling. *Nature* **426**, 570–574 (2003).
44. Gergely, F., Draviam, V. M. & Raff, J. W. The ch-TOG/XMAP215 protein is essential for spindle pole organization in human somatic cells. *Genes Dev.* **17**, 336–341 (2003).
45. Hood, F. E. et al. Coordination of adjacent domains mediates TACC3-ch-TOG-clathrin assembly and mitotic spindle binding. *J. Cell Biol.* **202**, 463–478 (2013).
46. Burgess, S. G., Bayliss, R. & Pfuhl, M. Solution NMR assignment of the cryptic sixth TOG domain of mini spindles. *Biomol. NMR Assign.* **9**, 411–413 (2015).
47. Fox, J., Howard, A., Currie, J., Rogers, S. & Slep, K. The XMAP215 family drives microtubule polymerization using a structurally diverse TOG array. *Mol. Biol. Cell* **25**, 2375–2392 (2014).
48. Lee, M. J., Gergely, F., Jeffers, K., Peak-Chew, S. Y. & Raff, J. W. Msps/XMAP215 interacts with the centrosomal protein D-TACC to regulate microtubule behaviour. *Nat. Cell Biol.* **3**, 643–649 (2001).
49. Vasquez, R. J., Gard, D. L. & Cassimeris, L. Phosphorylation by CDK1 regulates XMAP215 function in vitro. *Cell Motil. Cytoskeleton* **43**, 310–321 (1999).

Acknowledgements

We thank J. Shaevitz for help with image analysis, H. A. Stone for insightful discussions, M. Moritz for providing the γ-tubulin protein, S. Reber and P. Widlund for providing plasmids of XMAP215, M. Moritz, F. Hughson and S. Reber for critical reading of the manuscript and Petry laboratory members for discussions. Proteomics experiments were carried out by the Mass Spectrometry Core at Princeton University. A.T. thanks the Image Analysis course at MBL for useful training. This work was supported by the NIH New Innovator Award, Pew Scholars Program in the Biomedical Sciences, David and Lucile Packard Foundation (all to S.P.), American Heart Association predoctoral fellowship 17PRE33660328 (to A.T.) and the NIH post-doctoral fellowship 1F32GM119195-01 (to R.S.K.).

Author contributions

A.T. and S.P. conceived the project. A.T., R.S.K. and S.P. designed the experiments. A.T. and R.S.K. generated and characterized the reagents and tools. A.T. and R.S.K. performed and analysed all the experiments. A.T., R.S.K. and S.P. wrote the manuscript.

Competing interests

The authors declare no competing interests.

Additional information

Supplementary information is available for this paper at https://doi.org/10.1038/s41556-018-0091-6.

Reprints and permissions information is available at www.nature.com/reprints.

Correspondence and requests for materials should be addressed to S.P.

Publisher's note: Springer Nature remains neutral with regard to jurisdictional claims in published maps and institutional affiliations.

Methods

Purification of recombinant proteins. The wild-type XMAP215 with C-terminal green fluorescent protein (GFP) and seven histidine residues (GFP-7xHis) clone was a gift from S. Reber[26] and the TOG12-Kloop construct was from P. Widlund (TOG12+++)[24]. XMAP215 1-5AA-GFP-6xHis was synthesized (Genscript) and cloned into the pFastBac vector. The remaining XMAP215 constructs with C-terminal GFP-7xHis-Strep tags were cloned into the pST50Tr-STRHISNDHFR vector[50] using Gibson Assembly (NEB). The deletion constructs consisted of the following residues: TOG2-CT (264–2,065), TOG3-CT (544–2,065), TOG5-CT (1,091–2,065), TOG1-5 (1–1,460), TOG1-4 (1–1,090) and TOG1212 (1–543 + 1–515). Tubulin-binding mutants were derivatives of TOG1-5 or full-length XMAP215. Two residues in each TOG domain were mutated to alanine as described[24]. All constructs were fully sequenced.

Wild-type XMAP215-GFP and XMAP215 1-5AA were purified from Sf9 cells using the Bac-to-Bac system (Invitrogen). All other constructs were expressed in *Escherichia coli* Rosetta2 cells (Novagen) by inducing with 0.5–1 mM isopropyl-β-D-thiogalactoside (IPTG) for 12–16 h at 16 °C or 6–8 h at 25 °C. The cells were lysed (EmulsiFlex, Avestin) and the lysate was clarified by centrifugation at 13,000 r.p.m. in the Fiberlite F21-8 rotor (ThermoFisher) or at 65,000 r.p.m. in the Ti70 rotor (Beckman Coulter) for 30–45 min.

All proteins, except wild-type XMAP215 and TOG12-Kloop, were purified using Strep-affinity (Strep-Trap HP, GE Healthcare), followed either by gel filtration (HiLoad 16/600 Superdex, GE Healthcare) or dialysed into storage buffer. Wild-type XMAP215 was purified using His-affinity (His-Trap, GE Healthcare) and then cation exchange (Mono S 10/100 GL, GE Healthcare). TOG12-Kloop was purified as described previously[24]. His-GFP was purified using His-affinity. C-terminal GFP was replaced with a mCherry tag in the pET21a vector carrying EB1 (ref. [51]). EB1-mCherry was purified using His-affinity and dialysed into the CSF-XB buffer. Purifications of His-RanQ69L and glutathione *S*-transferase (GST)-tagged TPX2 α3-7 were described recently[52].

All proteins were dialysed into the CSF-XB buffer (100 mM KCl, 10mM K-HEPES, 5mM K-EGTA, 1 mM $MgCl_2$ and 0.1 mM $CaCl_2$, pH 7.7) with an additional 10% w/v sucrose, flash-frozen and stored at −80 °C. Protein concentrations were determined by analysing a Coomassie-stained SDS–PAGE against known concentrations of BSA (A7906, Sigma).

Antibodies. See Supplementary Table 1 for information on antibodies used in this study.

***Xenopus* egg extracts, immunodepletion and immunoprecipitation experiments.** CSF extracts were prepared from *Xenopus laevis* oocytes as described[53,54] and either used immediately or immunodepleted[51,53]. When working with *X. laevis*, all relevant ethical regulations were followed and all procedures were approved by Princeton Institutional Animal Care and Use Committee. For immunodepletions, XMAP215, TPX2, HAUS1 (a subunit of the augmin complex) or γ-tubulin and IgG (control) antibody were conjugated to Protein A Dynabeads (10002D, Life Technologies) overnight. Extracts (50–150 µl) were subjected to two sequential rounds of immunodepletion by incubating with roughly equal volume of antibody-conjugated bead slurry for 30–40 min in each round, as described previously[51,53]. See Supplementary Table 1 for antibody concentrations. The control immunodepletion was always performed, and the depletion efficiency was assessed using western blots and functional assays.

The immunoprecipitation experiment of XMAP215 and reciprocal immunoprecipitation of γ-TuRC (Supplementary Fig. 7a,b) was performed by coupling either XMAP215, γ-tubulin or Mzt1 antibody to Dynabeads. For immunoprecipitation of XMAP215, 75 µl of egg extracts were incubated with 125 µl of Dynabeads slurry for 1 h on ice. Beads were washed three times with five volumes of TBS buffer + 0.1% Tween20. For immunoprecipitation of γ-TuRC, 50 µl of extracts were incubated with 50 µl of Dynabeads slurry for 1 h at 4 °C, then washed twice with five volumes of CSF-XB buffer. Beads were boiled and the protein content was analysed using immunoblot (chemiluminescence) and imaged via X-ray film or iBright imaging system (ThermoFisher Scientific).

MT nucleation assays in *Xenopus* egg extracts. MT nucleation was assayed in *Xenopus* egg extracts as previously described[36,55]. Briefly, all reactions were performed with 0.5 mM vanadate (sodium orthovanadate, NEB) to avoid sliding of MTs. RanQ69L (5.5 µM) was added for branching nucleation experiments. For de novo nucleation reactions, an equal volume of buffer was added. MTs were labelled with 0.89 µM Cy5-labelled porcine brain tubulin and 200 nM EB1-mCherry (plus-tips). For testing activity of XMAP215 constructs (Figs. 5 and 6), 1 µM GST-tagged *X.l.* TPX2 α3-7 (ref. [36]) was also added to decrease the time lag until MT nucleation. For all experiments, either untreated extracts were used or endogenous XMAP215, TPX2, augmin or γ-tubulin was immunodepleted prior to use, and purified wild-type XMAP215 or XMAP215 constructs were added to the extract mixture at specified final concentrations. For Fig. 6, freshly purified proteins (TOG1-5, TOG12-Kloop and TOG5-CT) were used for comparing MT nucleation in extracts to in vitro polymerization (Fig. 6a); the same protein purification was used in both assays. The reaction mixture was prepared, incubated on ice for 2–3 min, 6 µl mixture was pipetted into a flow cell to start the reaction (timed as 0 s), and imaged for 15–20 min at 18–20 °C in a temperature-controlled room. All reagents added to extracts were stored in CSF-XB buffer, no more than 25% volumetric dilution of extracts was performed, and the reaction composition was kept constant for each experimental set. All reactions shown in individual figure panels were performed with one *Xenopus* extract preparation. TIRF imaging was performed with a Nikon TiE microscope using a 100×, 1.49 NA objective. Andor Zyla sCMOS camera was used for acquisition, with the field of view of 165.1 × 139.3 µm or 132.1 × 132.1 µm. Two × two binned, dual-colour images were acquired every 2 s using NIS-Elements software (Nikon). Brightness and contrast were optimized individually for display.

Analysis of MT nucleation in *Xenopus* egg extracts. The number of MTs and their growth speed in extracts were measured using a combination of custom-built and existing MATLAB software. EB1 intensity in the image sequence was homogenized by dividing a blank background image that was pre-blurred with Gaussian kernel of 20 pixels. For experiments in Figs. 1–3, immotile features were first discarded by applying a temporal median filter of 6–8 frames. EB1 comets were detected by comet detection and tracked by plus-end tracking module of uTrack[56,57]. An alternative pre-processing method was devised to analyse nucleation by XMAP215 constructs (Figs. 5 and 6) that was insensitive to growth speed or EB1 comet size, which varied between constructs. After background correction, EB1 comets were enhanced by applying a 2-pixel-wide Laplacian of Gaussian filter, followed by uTrack's comet detection process. MT nucleation curves were generated by plotting the number of EB1 comets detected or the number of EB1 tracks for each frame over time, as specified in each figure legend. For growth speed calculation, all EB1 tracks were classified into growth and forward gaps using uTrack's plus-end dynamics classification. Growth speed was measured from consecutive frames of growth events for all tracks.

De novo nucleation events and branched MT networks (Figs. 1f and 2b) were counted manually for the entire experimental duration or until a fixed time specified in the figure legends. The lifetime of MTs was measured manually for Supplementary Fig. 1d. Data regression to Michaelis–Menten kinetics or straight line was performed using the curve fit function in MATLAB.

Purification of γ-TuRC from *Xenopus* egg extracts. γ-TuRC purification was based on previous reports[5,17,58,59]. *Xenopus* egg extracts (10 ml) was diluted with five volumes of CSF-XBm buffer (CSF-XB buffer with 1 mM GTP, 1 mM dithiothreitol, and protease inhibitors and 10% w/v sucrose) and spun at 3,500 r.p.m. for 10 min to pellet large particles. GTP (1 mM) was added to all buffers and all steps were performed at 4 °C. The supernatant was diluted twofold with CSF-XBm buffer and filtered through a 0.22-µm filter. γ-TuRC was precipitated by the addition of 30% polyethylene glycol (PEG) solution to a final PEG concentration of 6.5%, incubated for 30 min, then centrifuged for 20 min at 17,500*g*. The PEG pellet was resuspended in 20 ml CSF-XBm buffer with 0.05% NP-40, the sample was centrifuged at 136,000*g* for 7 min and the supernatant was pre-cleared with Protein A Sepharose Beads (17127901, GE LifeSciences) for 20 min. Beads were removed, 1 ml γ-tubulin antibody (1 mg ml^{-1}) was added and the sample was incubated for 2 h with rotation. Washed Protein A Sepharose Beads (1 ml) were then added and incubated for 2 h. Beads containing bound γ-TuRC were centrifuged and the flow-through removed. Beads were washed three times with 10 ml CSF-XBm buffer + 0.05% NP-40, with 30 ml CSF-XBm + 250 mM KCl, 10 ml CSF-XBm + 1 mM ATP to remove heat-shock proteins, and finally with 10 ml CSF-XBm buffer. One millilitre of γ-tubulin peptide (residues 413–451) at 0.4 mg ml^{-1} in CSF-XBm buffer was incubated with beads overnight. After 10 h, additional CSF-XBm buffer was added and fractions 1–3 (1 ml each) were collected. For sucrose gradient fractionation, CSF-XBm buffer with 10% w/w sucrose instead and CSF-XBm with 50% w/w sucrose was layered in an ultra-clear 2.2-ml tube (11 × 34 mm, Beckman Coulter) and a continuous 10–50% sucrose gradient was made using the two-step program in the Gradient Master 108 machine. Peptide-eluted fractions were combined, concentrated, layered on top of the gradient and subjected to centrifugation at 200,000*g* in TLS55 rotor for 4 h. The gradient was fractionated from the top in 10–11 fractions and immunoblotted against GCP4, GCP5 and γ−tubulin to determine the γ-TuRC fractions.

Negative-stain electron microscopy. γ-TuRC sample (5 µl) was pipetted onto carbon grids and incubated at room temperature for 5 min. The grid was rinsed briefly in deionized water and 1% uranyl acetate was flowed over. Uranyl acetate was wicked away and the grid was air-dried. Images were taken on a CM100 TEM microscope.

Mass spectrometry. The peptide-eluted γ-TuRCs obtained were precipitated with trichloroacetic acid (TCA), resuspended in SDS buffer, separated by PAGE and stained with Coomassie dye. Gel bands were excised and analysed by the Mass Spectrometry Core facility at Princeton University. Gel bands were trypsin digested and peptides were analysed on Thermo Orbitrap Elite in the data-dependent mode with 120,000 MS1 resolution and up to 20 MS/MS scans in ion trap. Raw files were searched using Proteome Discoverer 2.1 (Thermo Scientific) with 10 p.p.m. MS1 and 0.5 Da MS2 tolerances. Caramidomethylation of cysteine was set as fixed modification, whereas oxidation of methionine, deamination of asparagine and conversion of glutamine to pyro-glutamate (at N termini) were set as dynamic

modifications. Data were searched against the *Xenopus* protein database defined in ref. [40], supplemented with common contaminant proteins. Scaffold 4.7.5 (Proteome Software) was used to validate MS/MS identifications. A protein false discovery rate of 1% and at least two peptides were accepted as confident protein identifications.

Nucleation assay with purified γ-TuRCs. Peptide-eluted γ-TuRCs were diluted twofold in BRB80 buffer (80 mM K-PIPES, 1 mM $MgCl_2$ and 1 mM EGTA, pH 6.8) to a final concentration of 3–6 nM GCP4 subunit, determined by quantitative immunoblot against purified, recombinant GCP4. Gradient fractionated γ-TuRCs were concentrated and exchanged into BRB80 using Amicon Ultra-4 ml 10,000 NMWL centrifugal filter unit. Bovine brain αβ-tubulin (Pursolutions) + 10% Alexa-568-labelled porcine brain tubulin, BRB80 buffer and 1.5 mM GTP were combined and clarified by centrifugation at 80,000 r.p.m. (TLA100.1 rotor, Beckman Coulter) for 20 min at 2 °C. The final tubulin concentration for each reaction ranged within 10–12 μM. MT nucleation was performed as described previously[5,17,58,60]. Clarified tubulin mixture was combined with γ-TuRCs with or without recombinant XMAP215 or TOG1-5 at described concentrations to 20 μl final volume on ice. The solution was incubated at 37 °C for 5 min, diluted with 80 μl warm BRB80 and the reaction was terminated with the addition of 100 μl of 2% glutaraldehyde in BRB80 buffer, then incubated at room temperature for 5 min. Samples were diluted 1:10 in BRB80, layered on top of 5-ml cushion of 20% glycerol in BRB80 buffer in a 15-ml Corex tube containing custom inserts to support round, poly-lysine-coated coverslips. The sample was centrifuged for 45 min at 25,000*g* in HB-6 rotor at 4 °C. Following centrifugation, MTs were fixed with ice-cold methanol, the coverslip mounted in Prolong Diamond solution and imaged via TIRF microscopy as described above. All images from each experimental set were taken in the same imaging session with constant TIRF angle, laser power and exposure.

The number of MTs in the entire field of view was counted manually and their total intensity was determined using a MATLAB script. Images were thresholded via Otsu method, eroded to eliminate tubulin aggregates having an aspect ratio of one and a mask for the MT signal was generated. The average intensity from the reverse mask was subtracted from the image as background. The residual fluorescent intensity per image was summed and reported.

In vitro MT polymerization. Coverslips and glass slides were coated with dichlorodimethylsilane[61]. Biotin-labelled, Alexa-594 and GMPCPP MTs were made as described[61], flash frozen and stored at −80 °C. Aliquots were thawed at 37 °C and diluted 2,000-fold in BRB80 buffer. The TIRF objective was warmed to 35 °C using an objective heater (model 150819-13, Bioptechs) prior to experiments.

Polymerization reactions were performed similar to previous reports[62]. Briefly, the flow chamber was incubated with anti-biotin antibody for 5 min, rinsed with BRB80 buffer, incubated with 1% Pluronic F127 in BRB80 for 5—10 min, rinsed again with BRB80 and incubated with diluted MT seeds for 10 min. The slide was protected from light. Unattached seeds were remove with BRB80 buffer + Trolox mix (2.5 mM PCA, 25 nM PCD and 2 mM Trolox)[63]. Attached seeds were visualized on the microscope. The polymerization mix (7.5 μM tubulin, 1 mg ml^{-1} κ-casein, 14.3 mM BME and 1 mM GTP in BRB80) was flowed in at room temperature to prime the channel, followed by the XMAP215 reaction mix (XMAP215 protein at the indicated concentration, 6.75 μM unlabelled bovine tubulin, 0.75 μM Cy5-labelled tubulin, 1 mg ml^{-1} κ-casein, 14.3 mM BME, 1 mM GTP and Trolox mix in BRB80). The chamber was immediately placed on the objective and imaged using the TIRF setup described above with the field of view of 132.1 × 132.1 μm. Single-colour images were obtained every 6 s, using 647-nm excitation (Cy5-dye) for 15 min, starting 2 min after the slide placement.

MT polymerization was analysed using ImageJ software. The maximum intensity projection of movie stacks was produced, and all polymerized MTs were marked using a region of interest generator. The stacks were resliced using the multi-kymograph plugin. The growth speed of the plus end was obtained as the slope of each kymograph.

MT polymerization in *Xenopus* egg extracts. Coverslips were passivated with dichlorodimethylsilane[61]. Biotin (20 μM) and Alexa-488-labelled, GMPCPP seeds were prepared fresh as described[23], digested with 0.2 mg ml^{-1} subtilisin A protease (P5380, Sigma) for 20 min at 37 °C. The digestion was stopped with 10 μM phenylmethylsulfonyl fluoride. MTs were pelleted for 20 min and resuspended in BRB80. Flow chambers were treated sequentially with anti-biotin antibody (10 min), BRB80 buffer, 500–1,000-fold dilution of subtilisin-digested seeds (10 min) and finally with CSF-XB buffer to remove unattached seeds. XMAP215 was depleted from egg extracts, and low concentrations of recombinant XMAP215-GFP was added back, along with 0.5 mM vanadate, 0.89 μM Cy5-tubulin and 200 nM EB1-mCherry. Extract mixture was added to the chamber containing subtilisin-digested seeds (timed as 0 s). Growth from most MT seeds was observed immediately (within 30–60 s). Imaging was completed within 300 s due to the disappearance of seeds by motors and slow degradation in extracts. TIRF imaging was performed as described above. Two × two binned, triple-channel images of Alexa-488 GMPCPP seeds (pseudocoloured as blue), EB1-mCherry (pseudocoloured as green) and Cy5-tubulin (red) were acquired every 3.5 s at 18–20 °C.

Growth speed was obtained by analysing composite kymographs of EB1 and tubulin intensity, as described above. The central, most-illuminated part of the movie stack was cropped (104 × 104 μm), GMPCPP seeds were observed roughly between 90 and 140 s from the start of reaction and the composite EB1 and tubulin signal was used to visually assess whether the observed GMPCPP seed had polymerized. For buffer add-back (0 nM XMAP215), the tubulin signal was not observed on all seeds, and this quantification was based on seeds where one end clearly showed EB1 spots associating, translating and dissociating in the movie stack (or EB1 blinking).

Size-exclusion chromatography experiments. Size-exclusion chromatography with γ-tubulin was performed as follows. All steps were performed at 4 °C. Purified, human γ-tubulin was a generous gift from M. Moritz in γ-TB buffer (defined as 50mM K-MES pH6.6, 5 mM $MgCl_2$, 1 mM EGTA, 10 mM thioglycerol and 10 μM GDP) with an additional 500 mM KCl and 10% glycerol. At high protein concentration, γ-tubulin forms large oligomers or filaments below physiological salt amounts[39]; thus, the salt concentration was reduced only when γ-tubulin concentration was simultaneously decreased. Small volumes (100–300 μl) of XMAP215 proteins were dialysed (69590, Life Technologies) into γ-TB buffer without salt or GDP for 2 h. After dialysis, protein aggregates were pelleted and the concentration was estimated using Bradford Reagent (Bio-Rad). γ-Tubulin was diluted to 280 nM in γ-TB buffer containing 220 mM KCl. γ-Tubulin and XMAP215 proteins were individually clarified by ultracentrifugation at 80,000 r.p.m. in TLA 100 (Beckman Coulter) for 15 min, then mixed in 1/1 volume ratio and incubated on ice for 10 min. The mixture (500 μl) was loaded onto the Superdex 200 Increase 10/300 column (GE Healthcare). The final concentration loaded to the column was 140 nM γ-tubulin and between 1 and 1.4 μM for most XMAP215 proteins, except XMAP215 FL 1-5AA at 0.7 μM. The column was equilibrated with γ-TB buffer containing 85 mM KCl and chromatography was performed in this buffer.

Size-exclusion chromatography experiments with αβ-tubulin were performed similar to previous reports[24]. Briefly, the Superdex 200 Increase 10/300 column was equilibrated with chromatography buffer. Bovine brain tubulin (Pursolutions) mixed with GTP and the XMAP215 construct were clarified individually as described above. For runs performed with the truncation constructs (Fig. 8a), final concentrations of 6.2 μM αβ-tubulin, TOG1-4 GFP (5 μM) and TOG5-CT GFP (6 μM) were used and chromatography was performed in αβ-TB buffer (25 mM Tris-HCl (pH 7.5), 75 mM NaCl, 1 mM $MgCl_2$, 1 mM EGTA and 1 mM BME) supplemented with 0.05% Tween20. For wild-type XMAP215-GFP runs (Supplementary Fig. 8d), αβ-TB buffer with 0.1% Tween20 was used for chromatography along with a final 4.4 μM tubulin and 4.3 μM XMAP215-GFP concentration. Runs in Supplementary Fig. 7c were performed in αβ-TB buffer containing either 75 mM NaCl (low salt concentration) or 150 mM NaCl (physiological salt concentration), both containing 0.025% Tween20, and XMAP215-GFP at 4.3 μM and tubulin at 4.4 μM were applied to the column. Each reaction was mixed to a final 0.2 mM GTP concentration, incubated on ice for 10 min and 100 μl was loaded onto the column.

For all control chromatography runs, an equal volume of corresponding buffer was used. Absorbance at 280 nm was recorded. High-molecular-weight gel filtration standards (thyroglobulin, aldolase and ovalbumin) were purchased from GE Healthcare (28403842) and used to estimate the Stoke's radii of eluted proteins in the same buffer that was used for the corresponding size-exclusion chromatography run[64]. For γ-tubulin size-exclusion chromatography experiments, 0.3-ml fractions were collected and alternate fractions eluted between 8.5 ml and 16.6 ml were analysed via immunoblot against γ-tubulin and GFP to detect XMAP215-GFP constructs. Secondary antibody conjugated to 800-nm IRDye (LI-COR) was used and imaged with the Odyssey CLx imaging station (LI-COR). For αβ-tubulin size-exclusion chromatography experiments, 0.2 ml fractions were collected and alternate fractions between 8.5 ml and 13.9 ml were analysed by SDS–PAGE stained with Coomassie dye.

In vitro immunoprecipitation with γ-tubulin. Immunoprecipitation was performed using a GFP tag on XMAP215 as the bait and γ-tubulin as the prey. Anti-GFP antibody was coupled to Protein A Dynabeads overnight. All proteins were pre-clarified via ultracentrifugation. XMAP215-GFP or the GFP tag at 500 nM was each mixed with 80 nM γ-tubulin in pulldown buffer (γ-TB buffer, as mentioned above, with a final 90 mM KCl and 0.04% Tween20 concentration). Empty beads (buffer) were used as an additional control without any GFP-tagged protein. One volume of Dynabeads was suspended in one volume each of immunoprecipitation mixture, incubated on a rotisserie for 1 h at 4 °C, then washed twice with five volumes of pulldown buffer. The protein content on the beads was analysed by immunoblot against γ-tubulin and GFP.

Statistics and reproducibility. All nucleation or polymerization experiments with *Xenopus* egg extracts were reproduced with at least three independent experiments, unless stated otherwise, with extracts freshly prepared from eggs laid by different animals on different days. Representative results are displayed or all data were reported, as specified in individual figure legends. Similar results were seen in all replicates that were performed. For in vitro polymerization,

at least two independent set of experiments were performed on different days with different protein purifications, where at least two replicates were completed for each purification. All results were pooled and reported and no difference was observed between different experimental sets. Nucleation experiments with purified γ-TuRCs were repeated at least three times, unless otherwise stated. Each replicate consisted of an independent preparation of γ-TuRC from different extract preparations. All results from the replicates showed similar results and were pooled and reported. All chromatography runs with γ-tubulin were repeated at least twice on different days with freshly prepared buffers and multiple protein purifications. Similar results were seen with all runs performed. Chromatography runs with αβ-tubulin were performed once with the exact buffer and at the exact concentration specified, with supporting runs performed in slightly varied conditions on different days with freshly prepared buffers and multiple protein purifications, as specified in the figure legends. Immunoprecipitation experiments in *Xenopus* extracts or in vitro were performed two to four times as indicated in the respective figure legends. All replicates showed similar results and the representative experiment was reported. No statistical tests were performed or reported.

Reporting Summary. Further information on experimental design is available in the Nature Research Reporting Summary linked to this article.

Code availability. MATLAB-based custom-built software in conjunction with open source software (uTrack, Danuser lab) was used for detecting and tracking EB1 particles. For other measurements and data analysis, MATLAB-based custom-built scripts were used. All codes are available from the authors upon request.

Data availability. Source data for Figs. 1e,f, 2b and 6b,d and Supplementary Figs. 2d,e, 4c,e and 6c have been provided as Supplementary Table 2. All data supporting the findings of this study are available from the corresponding author upon request.

References

50. Tan, S., Kern, R. C. & Selleck, W. The pST44 polycistronic expression system for producing protein complexes in *Escherichia coli*. *Protein Expr. Purif.* **40**, 385–395 (2005).
51. Petry, S., Pugieux, C., Nedelec, F. & Vale, R. Augmin promotes meiotic spindle formation and bipolarity in *Xenopus* egg extracts. *Proc. Natl Acad. Sci. USA* **108**, 14473–14478 (2011).
52. Alfaro-Aco, R., Thawani, A. & Petry, S. Structural analysis of the role of TPX2 in branching microtubule nucleation. *J. Cell Biol.* **216**, 983–997 (2017).
53. Hannak, E. & Heald, R. Investigating mitotic spindle assembly and function in vitro using *Xenopus laevis* egg extracts. *Nat. Protoc.* **1**, 2305–2314 (2006).
54. Murray, A. W. & Kirschner, M. W. Cyclin synthesis drives the early embryonic cell cycle. *Nature* **339**, 275–280 (1989).
55. King, M. & Petry, S. in *The Mitotic Spindle: Methods and Protocols* Vol. 1413 (eds Chang, P. & Ohi, R.) 77–85 (Humana, New York, 2016).
56. Applegate, K. T. et al. plusTipTracker: quantitative image analysis software for the measurement of microtubule dynamics. *J. Struct. Biol.* **176**, 168–184 (2011).
57. Jaqaman, K. et al. Robust single-particle tracking in live-cell time-lapse sequences. *Nat. Methods* **5**, 695–702 (2008).
58. Zheng, Y., Wong, M. L., Alberts, B. & Mitchison, T. Purification and assay of gamma tubulin ring complex. *Methods Enzymol.* **298**, 218–228 (1998).
59. Wiese, C. & Zheng, Y. A new function for the γ-tubulin ring complex as a microtubule minus-end cap. *Nat. Cell Biol.* **2**, 358–364 (2000).
60. Choi, Y. & Qi, R. Z. Assaying microtubule nucleation by the γ-tubulin ring complex. *Methods Enzymol.* **540**, 119–130 (2014).
61. Gell, C. et al. Microtubule dynamics reconstituted in vitro and imaged by single-molecule fluorescence microscopy. *Methods Cell Biol.* **95**, 221–245 (2010).
62. Zanic, M. Measuring the effects of microtubule-associated proteins on microtubule dynamics in vitro. *Methods Mol. Biol.* **1413**, 47–61 (2016).
63. Aitken, C. E., Marshall, R. A. & Puglisi, J. D. An oxygen scavenging system for improvement of dye stability in single-molecule fluorescence experiments. *Biophys. J.* **94**, 1826–1835 (2008).
64. Le Maire, M., Aggerbeck, L. P., Monteilhet, C., Andersen, J. P. & Moller, J. V. The use of high-performance liquid chromatography for the determination of size and molecular weight of proteins: a caution and a list of membrane proteins suitable as standards. *Anal. Biochem.* **154**, 525–535 (1986).

nature research

Corresponding author(s): Sabine Petry

Life Sciences Reporting Summary

Nature Research wishes to improve the reproducibility of the work that we publish. This form is intended for publication with all accepted life science papers and provides structure for consistency and transparency in reporting. Every life science submission will use this form; some list items might not apply to an individual manuscript, but all fields must be completed for clarity.

For further information on the points included in this form, see Reporting Life Sciences Research. For further information on Nature Research policies, including our data availability policy, see Authors & Referees and the Editorial Policy Checklist.

Please do not complete any field with "not applicable" or n/a. Refer to the help text for what text to use if an item is not relevant to your study.
For final submission: please carefully check your responses for accuracy; you will not be able to make changes later.

Experimental design

1. Sample size

Describe how sample size was determined.

No sample size calculation were performed and sample sizes were chosen with the following rationale for individual experiments.

For measuring nucleation in Xenopus egg extract, a number of samples were compared across each other. Each reaction was performed and observed for 15-20 minutes once in an experimental set due to limited lifetime of egg extract. During one reaction, a large field of view, roughly 140x140 um, was imaged that encompassed multiple branching networks containing 1000's of microtubules or 100's of de novo nucleated microtubules. The large numbers of microtubules measured in one field of view led to robust measurements above any noise. Before and after the experiment, the entire slide was scanned, which showed homogeneous distribution of networks across the slide. Therefore choosing one field of view for each reaction was representative and sufficient such that clear differences between samples were observed by imaging these large fields of view. The entire time-series was reported. The experimental results and trends were reproducible exactly, as indicated in respective figure legends.

For in vitro microtubule nucleation assays, a large coverslip was prepared with the sample. All fields of view (132x132um) were homogeneous and measurements from one field of view with another were consistent. 10-20 fields of view were imaged for each reaction to provide sufficient confidence in the measurements and results showed small error bars (plotted in respective figures) and clear patterns across various reactions performed. Therefore, 10-20 fields of sample size was sufficient to account for variation across fields and ensure reproducibility. The experimental results and trends were reproducible exactly from multiple experimental sets. Data from all experiments was pooled and reported.

For in vitro polymerization experiments, a large field of view (132x132um) was imaged for 15 minutes, usually containing more than 20 microtubule templates. Growth speed from more than 20 microtubule templates was obtained for every concentration of each protein construct. Before and after the experiment, the entire slide was scanned, which showed homogeneous distribution of microtubules and growths across the slide. The experiments performed on different days with different batches of purified protein, which resulted in the exact agreement in measurements across each other. The measurements were reproducible, and therefore 20 measurements for each reaction was sufficient. Data from all experiments was pooled and reported.

For chromatography, each run was performed once in an experimental set and shift of proteins due to binding was observed. Clear shift of g-tubulin or alpha/beta-tubulin signal was observed in each experiment, showing clear interaction or no interaction. In some experimental sets, repeat of one reaction was performed and gave the same results. Therefore, one reaction for each condition for every experiment was sufficient. Sets of chromatography runs were repeated on different days using different protein preparations and freshly made buffers. The repeats resulted in an exact agreement.

For immunoprecipitation experiments in vitro and in Xenopus egg extracts, the set of precipitations indicated in the figures were performed simultaneously and at the same concentrations across samples. Clear signal of prey protein(s) was observed using immunoblots in each experiment, showing clear binding or no binding. In certain experiments, the same immunoprecipitation reaction was repeated and gave the same result, therefore, one sample for each reaction within an experimental set was sufficient. The experimental set was repeated and similar results were observed, as described in figure

legends.

All experiments performed in this work were repeated at least three times, unless indicated otherwise in individual figure legends. All repeats performed resulted in exact agreement or similar results.

2. Data exclusions

Describe any data exclusions.

No data was excluded in experiments or analyses.

3. Replication

Describe the measures taken to verify the reproducibility of the experimental findings.

For experiments performed in Xenopus egg extract, each experimental set was repeated with at least 3 independent extract preparations, unless indicated otherwise. Each experiment was performed from independent extract preparations, i.e. on different days using freshly laid eggs from different animals and with freshly made buffers. Similar results or exact agreement was seen across all repeats.

For in vitro microtubule nucleation assays with purified g-TuRC, fresh g-TuRC protein was prepared using freshly made buffers and Xenopus egg extracts obtained from different animals for each experimental set. These experiments were repeated at least two-three times as indicated in respective figure legends, with additional supporting experimental sets. Similar results were seen across all g-TuRC preparations.

For in vitro polymerization, two sets of experiments were performed on different days with fresh protein purifications and fresh buffers for each experiments. Multiple replicates were performed on individual purifications as well in one day. No difference was observed between any repeats.

For size exclusion chromatography with gamma-tubulin, at least 2 independent runs were performed on different days with each XMAP215 construct, using freshly made buffers. Multiple supporting runs were also performed with multiple protein preparations, as described in individual figure legends. For size exclusion chromatography with alpha/beta-tubulin, 1 experimental run at the reported buffer and protein concentrations was performed and multiple supporting experiments were performed on different days with fresh buffers and multiple protein purifications, as described in respective figure legends. Exact agreement was seen across all repeats.

Immunoprecipitation experiments were repeated on different days, with freshly prepared egg extracts or buffers (independent experiments) two to four times as indicated in individual figure legends. Similar results were seen across all repeats.

All experimental repeats resulted in exact agreement or similar results across all experiments. Extensive details on statistics and reproducibility are reported in respective figure legends and "Statistics and Reproducibility" section of Methods section.

4. Randomization

Describe how samples/organisms/participants were allocated into experimental groups.

Randomization was not relevant for this study, as samples were never needed to be distributed into experimental groups. Experiments in Xenopus egg extracts were performed on one tube of Xenopus egg extract prepared fresh on the day and no allocation of sample was needed. For all other experiments, purified proteins were used that were from the same batch of purification for every experimental set, and no allocation was required. Therefore, no randomization was performed.

5. Blinding

Describe whether the investigators were blinded to group allocation during data collection and/or analysis.

Investigators were not blinded to data collection and analyses.

DATA COLLECTION
With Xenopus egg extracts, on one tube of Xenopus egg extract prepared fresh on the day and purified proteins either at different concentrations or different protein constructs were added. The imaging was performed by the investigators during the experiment, therefore blinding was not possible. For in vitro polymerization, again, purified proteins either at different concentrations or different protein constructs were added. The imaging was performed by the investigators during the experiment, therefore blinding was not possible. For in vitro nucleation and size exclusion chromatography, the experiments were performed in a series and their data was collected in a batch, either through microscopy or SDS-PAGE or immunoblot analysis on a later day, therefore blinding during the experimentation was not required. For the in vitro nucleation reactions, the difference between absence or presence of g-TuRC was so dramatic that blinding to the sample was not possible during image acquisition. Similarly, during data collection for chromatography, the presence or absence of interaction was very clear, and blinding to the sample was not possible during acquisition.

DATA ANALYSES
Most analyses performed in Xenopus egg extracts was done via automated image analyses software for nucleation measurements and growth speed without investigators' interference.

Therefore, blinding was not required. Similarly, total microtubule mass measurement in g-TuRC nucleation assay was performed via automated MATLAB scripts and blinding was not required. For counting microtubules in vitro (S4C, S6C) or Xenopus egg extracts (1F, 2B), all microtubules were meticulously counted by the investigators and blinding was not performed.

Thus, for this study, blinding was either not required during the experiments or analyses, or not performed since data was collected by the investigators.

Note: all in vivo studies must report how sample size was determined and whether blinding and randomization were used.

6. Statistical parameters

For all figures and tables that use statistical methods, confirm that the following items are present in relevant figure legends (or in the Methods section if additional space is needed).

n/a	Confirmed
☐	☒ The exact sample size (*n*) for each experimental group/condition, given as a discrete number and unit of measurement (animals, litters, cultures, etc.)
☐	☒ A description of how samples were collected, noting whether measurements were taken from distinct samples or whether the same sample was measured repeatedly
☐	☒ A statement indicating how many times each experiment was replicated
☒	☐ The statistical test(s) used and whether they are one- or two-sided *Only common tests should be described solely by name; describe more complex techniques in the Methods section.*
☒	☐ A description of any assumptions or corrections, such as an adjustment for multiple comparisons
☒	☐ Test values indicating whether an effect is present *Provide confidence intervals or give results of significance tests (e.g. P values) as exact values whenever appropriate and with effect sizes noted.*
☐	☒ A clear description of statistics including central tendency (e.g. median, mean) and variation (e.g. standard deviation, interquartile range)
☐	☒ Clearly defined error bars in all relevant figure captions (with explicit mention of central tendency and variation)

See the web collection on statistics for biologists for further resources and guidance.

Software

Policy information about availability of computer code

7. Software

Describe the software used to analyze the data in this study.

MATLAB-based custom-built software in conjunction with open source software (Plus-tip tracker in uTrack 2.1.3, Danuser group) were used for detecting and tracking EB1 particles in Xenopus egg extract. For other measurements and data analysis, MATLAB-based custom-built scripts were used. All codes with detailed instructions on their use are available from the authors upon request.

For building kymographs for growth speed measurements (Fig. 6A and Supp Fig. 2D), ImageJ software was used with inbuilt multi-kymograph plugin.

For mass spectrometric analysis of g-TuRC purification, Proteome Discoverer 2.1 and Scaffold 4.7.5 softwares were used by the Mass Spectometry Core at Princeton University.

For manuscripts utilizing custom algorithms or software that are central to the paper but not yet described in the published literature, software must be made available to editors and reviewers upon request. We strongly encourage code deposition in a community repository (e.g. GitHub). *Nature Methods* guidance for providing algorithms and software for publication provides further information on this topic.

Materials and reagents

Policy information about availability of materials

8. Materials availability

Indicate whether there are restrictions on availability of unique materials or if these materials are only available for distribution by a third party.

All materials along with detailed instructions on their use are available from the authors upon request.

9. Antibodies

Describe the antibodies used and how they were validated for use in the system under study (i.e. assay and species).

Detailed information on antibodies used in this study can be found in Supplementary Table 1. Commercial antibodies were validated as noted on manufacturer's website and with our tests performed in the lab, as described in the Supplementary Table 1.

10. Eukaryotic cell lines

a. State the source of each eukaryotic cell line used.

No cell lines were used in this manuscript.

b. Describe the method of cell line authentication used.

As no cell lines were used, no cell line authentication was needed or performed.

c. Report whether the cell lines were tested for mycoplasma contamination.

Because no cell lines were used, cell lines were not tested for mycoplasma contamination.

d. If any of the cell lines used are listed in the database of commonly misidentified cell lines maintained by ICLAC, provide a scientific rationale for their use.

No cell lines were used in this study, so no cell lines were found in the database of commonly misidentified cell lines that is maintained by ICLAC and NCBI Biosample.

Animals and human research participants

Policy information about studies involving animals; when reporting animal research, follow the ARRIVE guidelines

11. Description of research animals

Provide all relevant details on animals and/or animal-derived materials used in the study.

Mitotic extracts were prepared from Xenopus laevis oocytes. Mature, female frogs (age 2-7 years) were used. All experiments were performed in compliance with IACUC protocols and guidelines.

Policy information about studies involving human research participants

12. Description of human research participants

Describe the covariate-relevant population characteristics of the human research participants.

The study did not involve human research participants.